



Transgenic mice for in vivo epigenome editing with CRISPR-based systems

Matthew P. Gemberling^{1,2,13}, Keith Siklenka^{2,3,13}, Erica Rodriguez^{0,4}, Katherine R. Tonn-Eisinger^{0,4}, Alejandro Barrera^{0,2,3}, Fang Liu⁴, Ariel Kantor^{1,2}, Liqing Li³, Valentina Cigliola^{5,6}, Mariah F. Hazlett⁴, Courtney A. Williams³, Luke C. Bartelt^{2,3}, Victoria J. Madigan^{0,7}, Josephine C. Bodle^{1,2}, Heather Daniels^{1,2}, Douglas C. Rouse⁸, Isaac B. Hilton^{0,1,11,12}, Aravind Asokan^{1,2,6,7,9}, Maria Ciofani^{2,10}, Kenneth D. Poss^{0,2,5,6}, Timothy E. Reddy^{0,2,3}, Anne E. West^{0,2,4} and Charles A. Gersbach^{0,1,2,5,6,7} ⋈

CRISPR-Cas9 technologies have dramatically increased the ease of targeting DNA sequences in the genomes of living systems. The fusion of chromatin-modifying domains to nuclease-deactivated Cas9 (dCas9) has enabled targeted epigenome editing in both cultured cells and animal models. However, delivering large dCas9 fusion proteins to target cells and tissues is an obstacle to the widespread adoption of these tools for in vivo studies. Here, we describe the generation and characterization of two conditional transgenic mouse lines for epigenome editing, Rosa26:LSL-dCas9-p300 for gene activation and Rosa26:LSL-dCas9-KRAB for gene repression. By targeting the guide RNAs to transcriptional start sites or distal enhancer elements, we demonstrate regulation of target genes and corresponding changes to epigenetic states and downstream phenotypes in the brain and liver in vivo, and in T cells and fibroblasts ex vivo. These mouse lines are convenient and valuable tools for facile, temporally controlled, and tissue-restricted epigenome editing and manipulation of gene expression in vivo.

pigenome editing with CRISPR-Cas9 systems has become a widespread approach for investigating fundamental aspects of biological processes through the targeted regulation of genes and the non-coding genome1. Fusion of the nuclease-deactivated Cas9 (dCas9) to transcriptional activator or repressor domains enables targeted manipulation of gene expression. Initial work to characterize dCas9 fused to the tetramer of the VP16 acidic activation peptide (dCas9VP64) laid the framework for the development of a wide range of next-generation transcriptional activators, including SAM, VPR, p300core, Tet1CD and others²⁻⁹. In addition, dCas9 fusions that can repress gene expression have been characterized as functioning through direct or indirect chromatin modification using domains and enzymes such as KRAB, MECP2 and DNMT3a (refs. ^{2,10,11}). In particular, we and others have shown that dCas9^{p300} and dCas9KRAB can be targeted to enhancers or to positions near transcriptional start sites (TSSs), leading to targeted histone acetylation or methylation and subsequent changes in gene expression^{3,12}. These epigenome-modifying dCas9 fusion proteins have been used for studies of gene regulation^{13–15}, directed cell differentiation^{16–20}, therapeutic gene modulation^{21,22}, and high-throughput screening of putative gene regulatory elements^{23–26}.

Although the majority of studies using CRISPR-based epigenome editing tools have focused on ex vivo cell culture systems, in which delivery challenges are readily addressable, there are several examples of the powerful utility of targeted gene activation and repression in vivo. The smaller dCas9 from *Staphylococcus aureus*²⁷

was incorporated into a dCas9KRAB fusion protein and delivered with a guide RNA (gRNA) expression cassette via adeno-associated virus (AAV) for targeted gene repression in the mouse liver²¹. Short 'dead' gRNAs were used to activate gene expression in the liver and muscle of the Cas9 transgenic mouse²⁸ using AAV co-delivery of these gRNAs with an MPH activator module²⁹. A dCas9-SunTag transgenic mouse has been used to activate gene expression in the midbrain³⁰ and liver³¹. Another study used a constitutively expressed dCas9VP64 knock-in to activate expression of the Sim1 gene and reverse obesity resulting from Sim1 haploinsufficiency when crossed to mice transgenic for gRNA expression cassettes²². Although most of the previous studies have focused on gene activation, one recent study generated a tetracycline-inducible dCas9KRAB mouse line. Hematopoietic stem cells from this line were then engineered ex vivo to assess the impact of five transcription factors on hematopoietic lineage determination after transplantation into a host animal³². Plasmids encoding either dCas9^{VP64} or dCas9^{KRAB} have also been transfected into the mouse brain to investigate the role of epigenetic regulation in addiction behaviors13.

These experiments highlight the potential of CRISPR-based epigenome editing in studies of gene regulation. Accordingly, we sought to generate widely applicable transgenic mouse lines to readily perform temporally controlled and tissue-restricted epigenome editing for both gene activation and repression with the simple addition of the gRNA. There are several potential advantages to using Cre-inducible expression of dCas9-based epigenome editors from

¹Department of Biomedical Engineering, Duke University, Durham, NC, USA. ²Center for Advanced Genomic Technologies, Duke University, Durham, NC, USA. ³Department of Biostatistics and Bioinformatics, Duke University School of Medicine, Durham, NC, USA. ⁴Department of Neurobiology, Duke University School of Medicine, Durham, NC, USA. ⁵Department of Cell Biology, Duke University Medical Center, Durham, NC, USA. ⁶Regeneration Next Initiative, Duke University, Durham, NC, USA. ⁷Department of Surgery, Duke University Medical Center, Durham, NC, USA. ⁸Division of Laboratory Animal Resources, Duke University School of Medicine, Durham, NC, USA. ⁸Department of Molecular Genetics and Microbiology, Duke University Medical Center, Durham, NC, USA. ¹⁰Department of Immunology, Duke University Medical Center, Durham, NC, USA. ¹¹Present address: Department of Biosciences, Rice University, Houston, TX, USA. ¹³These authors contributed equally: Matthew P. Gemberling, Keith Siklenka. ⁵²e-mail: charles.gersbach@duke.edu

transgenic mouse lines compared with viral delivery. First, several epigenome editors, such as dCas9 fusions to the acetyltransferase p300, are too large for viral vectors. Second, a single genomic copy ensures a more uniform expression level between cells and animals. Third, the use of a genetically encoded Cre recombinase adds tissue or cell type specificity when a corresponding promoter that can be packaged into viral vectors is unavailable. Fourth, it is possible to genetically encode both the gRNA and the Cre recombinase to alter gene expression or program epigenetic states in cell types that are not readily transduced by viral vectors. And last, the transgenic expression of dCas9-based epigenome editors may overcome challenges associated with immune system recognition of the bacterial Cas9 protein^{33–37}. Here, we characterize and demonstrate the utility of two mouse lines, Rosa26-LSL-dCas9-p300core (dCas9p300) and Rosa26-LSL-dCas9-KRAB (dCas9KRAB), for in vivo epigenome editing and modulation of gene expression.

Results

Generation and characterization of the mouse lines. We generated dCas9 epigenome editor mice by inserting a Cre-inducible cassette into the Rosa26 locus using traditional homologous recombination in mouse embryonic stem cells (Fig. 1a). The inserted transgene consists of a CAG promoter followed by a *loxP*-stop-*loxP* (LSL) cassette, followed by the complementary DNA encoding the dCas9 fusion protein containing a FLAG epitope. This allows for inducible expression of the dCas9 fusion protein in response to Cre recombinase activity that results in removal of the stop signal between the *loxP* sites. To evaluate the inducibility of the dCas9^{p300} and dCas9^{KRAB} lines, we treated the mice with AAV9:CMV.Cre and found Cre-dependent expression in the spleen, skeletal muscle, liver, pancreas and heart (Supplementary Figs. 1 and 9b).

Targeted gene activation in the liver. To demonstrate activation of gene expression with dCas9 p300 in cells harboring a single genomic insertion of the dCas9 p300 expression cassette, we isolated primary fibroblasts from the gastrocnemius and tibialis anterior hind limb muscles of the dCas9 p300 mouse to test gRNAs in cell culture. We tested four gRNAs targeting the TSS of Pdx1 (pancreatic and duodenal homeobox 1) (Supplementary Fig. 2a). Pdx1 was originally selected as a target due to its ability to induce liver cells to develop into a pancreatic β-cell-like phenotype, including glucose-responsive insulin expression³⁸. Cells were co-transduced with lentiviral vectors encoding Cre and a single gRNA expression cassette and cultured for 4d, at which point RNA was isolated for gene expression analysis using quantitative polymerase chain reaction with reverse transcription (RT–qPCR). Two of the four gRNAs significantly increased Pdx1 messenger RNA levels compared with

a control gRNA targeting *Myod*. For all future experiments, we continued with gRNA no. 4 given that it showed the greatest activation of *Pdx1* mRNA expression, at an ~150-fold increase relative to controls (Supplementary Fig. 2b).

This Pdx1-targeting gRNA was cloned into an AAV vector containing a ubiquitous CBh promoter driving Cre (AAV9:Cbh. Cre-Pdx1.gRNA), which we injected into 8-week-old mice, from which we then collected liver tissue 2 weeks later to assess Pdx1 mRNA expression (Fig. 1b). The *Pdx1* mRNA levels were increased several thousandfold compared with treatment with a corresponding AAV vector containing a non-targeting control gRNA (Fig. 1c). We confirmed an increase in PDX1 protein levels in tissue sections of the livers treated with the Pdx1-targeting gRNA compared with those treated with the non-targeting gRNA control as measured with immunofluorescence staining (Fig. 1d). In the animals treated with Pdx1 gRNA, 7.0% of nuclei were PDX1 positive, compared with 0.03% of cells in livers treated with the control gRNA (Fig. 1e). However, we did not detect an increase in insulin mRNA using RT-qPCR or protein using immunostaining in any treated animals. This result is supported by previous studies showing that hyperactive PDX1-VP16 overexpression is necessary to achieve robust insulin induction39.

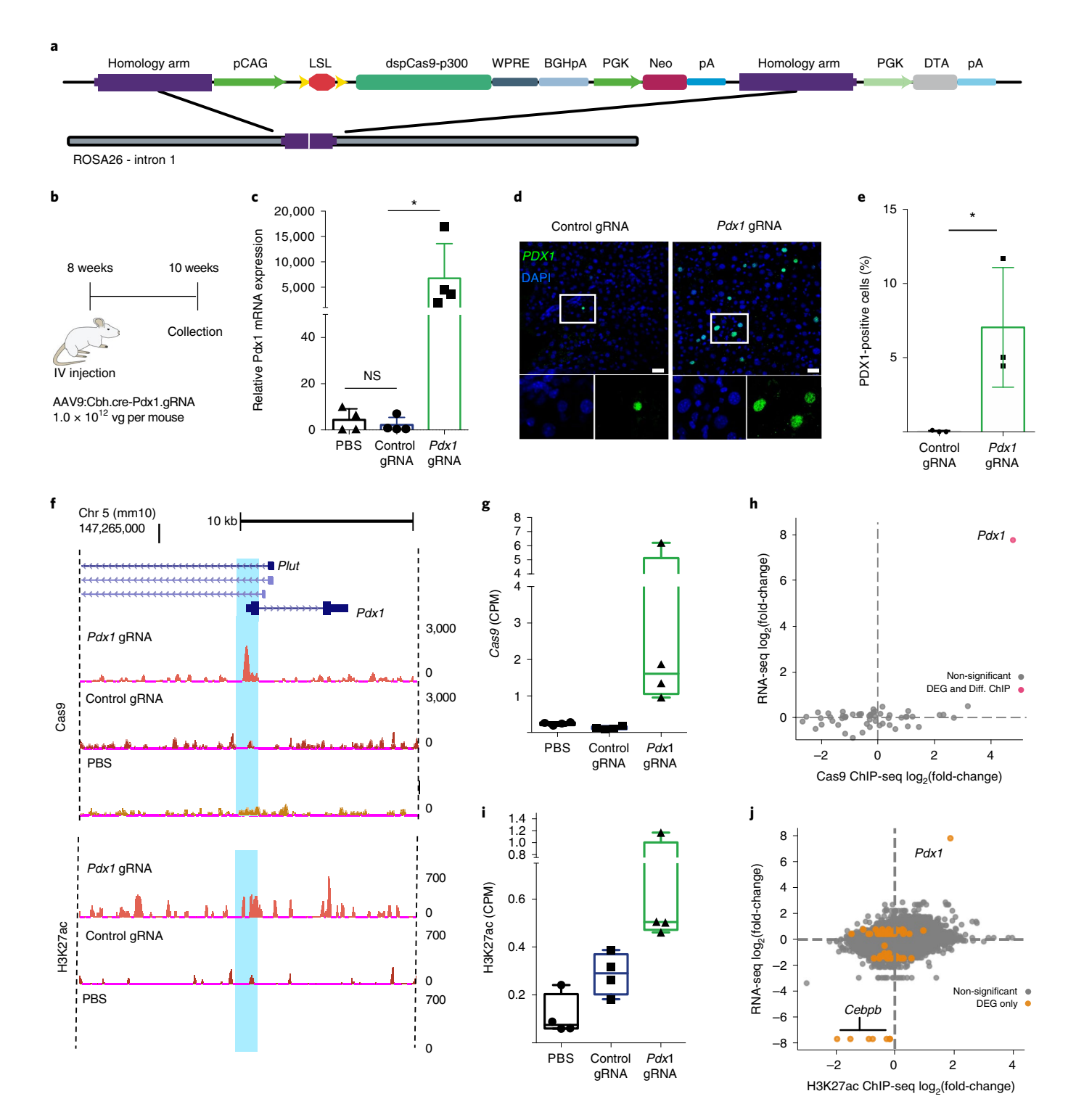
After demonstrating robust target gene activation, we characterized the specificity of gene regulation in the dCas9p300 mice. Although the p300 acetyltransferase has many well-characterized targets involved in gene regulation, previous studies showed deposition of acetylation of lysine 27 on histone subunit 3 (H3K27ac) in regions of dCas9^{p300} binding that is concomitant with an increase in target gene mRNA levels^{3,14,19,40-43}. To assess the genome-wide specificity of both dCas9 binding and targeted acetylation, we performed chromatin immunoprecipitation and sequencing (ChIP-seq) using antibodies against dCas9 and H3K27ac. Significant levels of specific binding of dCas9p300 to the targeted region of Pdx1 (Fig. 1f,g and Supplementary Fig. 3) and increased H3K27ac in the surrounding regions were readily detectable (Fig. 1f and Supplementary Fig. 4). Genome-wide comparisons showed that the only significantly different dCas9 binding site between treatment with the Pdx1-targeting gRNA and that with the non-targeting gRNA controls was at the Pdx1 gRNA target site (Fig. 1h). Genome-wide, H3K27ac levels were not significantly different between the Pdx1-targeting gRNA and non-targeting gRNA control treatments (Supplementary Fig. 5a). However, we observed a twofold increase in H3K27ac at the Pdx1 gRNA target binding site as compared with the non-targeting control gRNA (Fig. 1i). Comparing the mice injected with AAV encoding Cre and the Pdx1-targeted gRNA with the control mice injected with saline, we found widespread differential H3K27ac levels, which appears to be attributable to gRNA-independent

Fig. 1| AAV-based gRNA and Cre recombinase delivery to Rosa26:LSL-dCas9^{p300} mice activates Pdx1 gene expression and catalyzes targeted histone acetylation. a, Schematic diagram of the dCas9p300 knock-in locus. BGH, bovine growth hormone. b, Schematic diagram of the experiment for in vivo Pdx1 activation. vg, vector genomes. c, Pdx1 mRNA quantification 2 weeks after injection in liver tissue lysates isolated from mice injected with PBS, or AAV9 encoding Cre and either a control non-targeting or Pdx1-targeting gRNA (n=4 per group, Kruskal-Wallis one-way ANOVA with Dunnett's post-hoc test, *P=0.0132). d, PDX1 immunostaining of liver tissue sections at 14 d after injection of mice treated with control and Pdx1-targeted gRNAs. Scale bars, 50 μm. **e**, Quantification of PDX1-positive nuclei in control gRNA- and Pdx1 gRNA-treated animals (7.0% versus 0.03%, P = 0.019, Student's t-test, n = 3 animals, with 3 images counted per animal). f, Representative browser tracks of dCas9 and H2K27ac ChIP-seq data from treated livers at 2 weeks after treatment. Chr-5 (mm10), chromosome 5 (Genome Reference Consortium Mouse Build 38). g, dCas9 ChIP-seq quantification of sequencing counts (CPM, counts per million) in the gRNA target region of Pdx1 in samples from mice treated with Pdx1-targeted gRNA, control gRNA or PBS (n=4, one-way ANOVA with Dunnett's post-hoc test, P=0.059). h, RNA-seq and Pdx1 ChIP-seq analyses showing the relationship between changes in gene expression and occupancy of dCas 9^{p300} genome-wide (n=4, FDR < 0.05). i, H3K27ac ChIP-seq quantification of sequencing counts in a 1kb window centered on the gRNA target site near the TSS of Pdx1 in samples from mice treated with the Pdx1-targeted gRNA, control gRNA or PBS (n=4, two-tailed Student's t-test, P=0.07). j, RNA-seq and H3K27ac ChIP-seq analysis showing the relationship between changes in gene expression and genome-wide H3K27 acetylation for samples from mice treated with the Pdx1-targeted gRNA and control gRNA (n=4, FDR < 0.05). Cebpb, CCAAT enhancer-binding protein-β. DEG, differentially expressed gene (orange dot); Diff. ChIP, differentially enriched ChIP-seq signal (blue dot); DEG and Diff. ChIP, differentially expressed gene and ChIP-seq enrichment (red dot). All bar-plot error bars represent standard deviation, and all boxplots are drawn from the 25th to 75th percentile with the horizontal bar at the mean and the whiskers extending to the minima and maxima.

consequences of overexpression of the constitutively active p300 acetyltransferase catalytic domain (Supplementary Fig. 5d).

To assess the specificity of changes in gene expression downstream of targeted histone acetylation, we performed RNA sequencing (RNA-seq) on mRNA collected from treated mouse livers. When compared with treatment with Cre and a non-targeting gRNA, the *Pdx1*-targeted gRNA led to increases in *Pdx1* expression that were the greatest change in gene expression transcriptome-wide (Fig. 1h,) and Supplementary Figs. 5g and 6a). This is consistent with previous levels of specificity reported for dCas9^{p300} in cultured cells³. However, when comparing *Pdx1*-targeting gRNA or control non-targeting gRNA with saline-injected controls, we observed widespread gRNA-independent changes in gene expression as a result of dCas9^{p300} expression (Supplementary Fig. 6b,c). These results support gRNA-mediated specific epigenome editing and changes to target gene expression in vivo in this dCas9^{p300} mouse, but also underscore the need for proper controls to account for gRNA-independent effects when overexpressing constitutively active catalytic domains of epigenome editors.

Targeted gene activation in the brain. To test gene activation in differentiated neurons with a single genomic insertion of the dCas9^{p300}



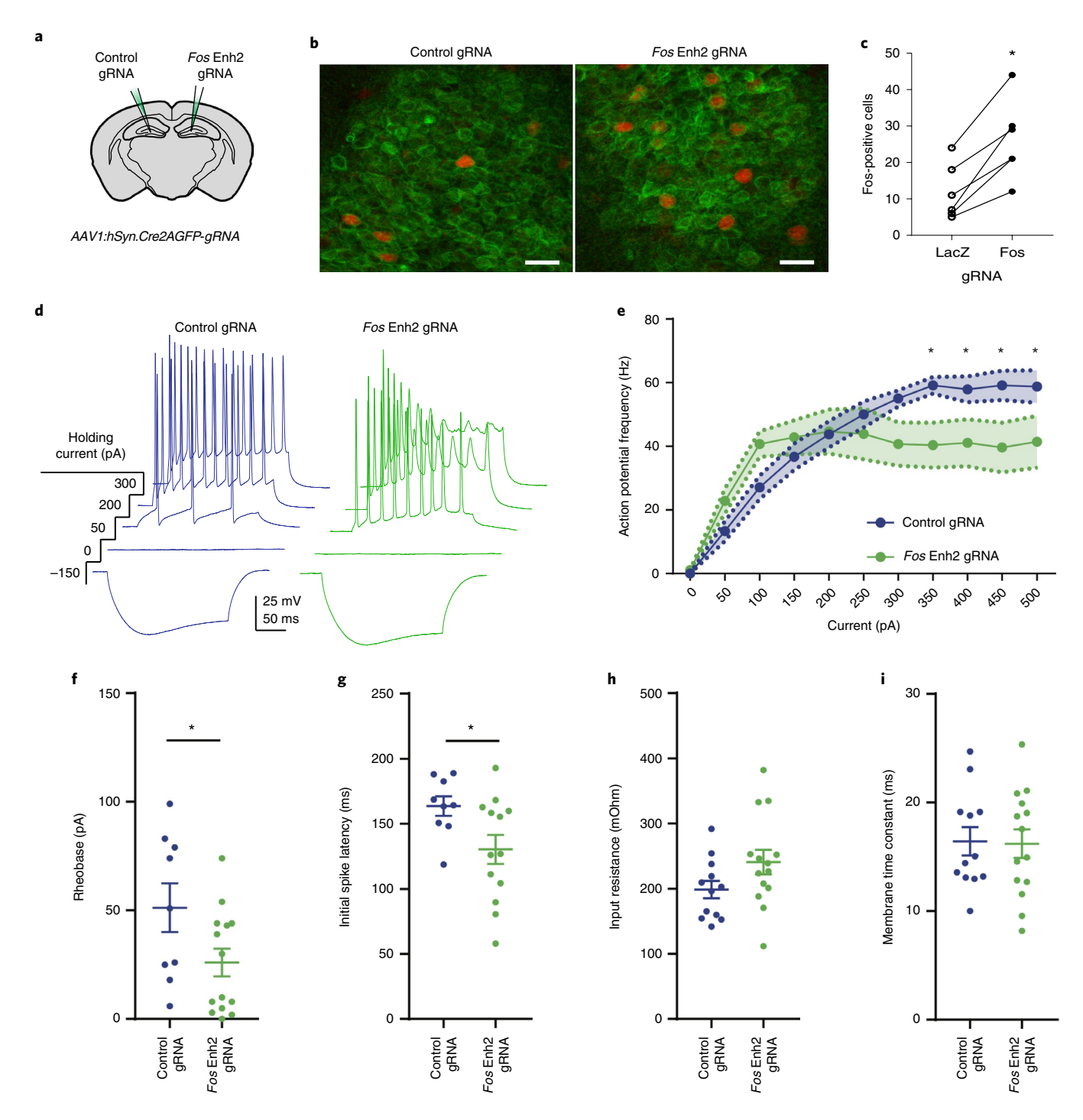


Fig. 2 | Epigenomic enhancement of *Fos* **in vivo increases excitability in CA1 neurons. a**, Contralateral AAV injection strategy for comparison of targeting and non-targeting control gRNAs. **b**, Immunofluorescence imaging of neurons in the dentate gyrus region of the hippocampus after transduction with AAV containing LacZ control gRNA or Fos Enh2 gRNA and stimulation with novel objects. AAV-gRNA-positive neurons, green; FOS-positive neurons, red. Scale bars, 20 µm. **c**, Quantification of those FOS-positive neurons in **b**. The lines connect measurements from the two sides of the same mouse, and the counts are of FOS-positive cells in tissue slices from n = 6 paired ROIs per condition from 3 animals. *P = 0.002 (Student's paired two-sided t-test). **d**, Representative current-clamp traces from acute hippocampal slices. **e**, Action potential stimulus-response curves for neurons expressing Fos Enh2 gRNA compared with neurons expressing the LacZ control gRNA. Current, F(10,240) = 31.12 (P < 0.0001); virus, F(1,24) = 1.05 (P = 0.32); current × virus interaction, F(10,240) = 4.64 (P < 0.0001). The difference between Fos Enh2 gRNA (n = 14) and the LacZ control gRNA (n = 12) at 350 pA (P = 0.016), at 400 pA (P = 0.031), at 450 pA (P = 0.012) and at 500 pA (P = 0.026) was significant (two-way repeated measures ANOVA with post-hoc Fisher's LSD test; *P < 0.05, the error band represents the s.e.m.). **f-i**, The rheobase (P = 0.023) (**f**) and the latency to first spike (P = 0.018) (**g**) were significantly lower for the neurons expressing Fos Enh2 gRNA compared with the LacZ controls, but the input resistance (P = 0.092) (**h**) and the membrane time constant (P = 0.091) (**i**) were not significantly different. LacZ control gRNA, n = 12; Fos Enh2 gRNA, n = 14; each from 2 animals (two-tailed Student's t-test; horizontal bars represent the mean; error bars show the s.e.m.).

expression cassette, we first sought to regulate gene expression in cultured primary neurons. Previously, we showed that gRNA-mediated recruitment of dCas9VP64 over-expressed from a lentiviral vector is sufficient to drive expression of the mature neuronal NMDA receptor subunit Grin2c in developing cerebellar granule neurons (CGNs)¹⁵. Here, to determine whether the Cre-inducible dCas9^{p300} transgene is similarly effective for activating gene expression, we cultured CGNs heterozygous for the dCas9p300 transgene and then either induced dCas9p300 expression by lentiviral delivery of Cre or over-expressed dCas9VP64 from a lentiviral vector for comparison. Recruitment of dCas9p300 to the Grin2c promoter activated Grin2c expression to a similar degree to that by dCas9VP64 recruitment (Supplementary Fig. 7a). This activation was specific for Grin2c and was not due to accelerated neuronal maturation because the expression of another developmentally upregulated gene, Wnt7a, was not different in any of the conditions (Supplementary Fig. 7b). In addition, these data suggest that the dCas9p300 transgene is at least as effective as lentiviral dCas9VP64 for inducing expression of developmental genes in cultured primary neurons.

To determine the ability of transgenic dCas9^{p300} to regulate gene expression in neurons in vivo, we measured the induction of neuronal activity-dependent genes in the hippocampus, a brain region that is important for spatial learning and memory. Fos transcription is rapidly and robustly induced by the physiological changes in neuronal firing that follow sensory experience. The Fos gene is flanked by five enhancer elements that regulate its stimulus-dependent transcription. We previously showed that expression of dCas9p300 from a transfected plasmid and its recruitment to enhancer 2 (Enh2) is sufficient to increase Fos mRNA and protein expression levels in cultured neurons14. To recruit dCas9p300 to Enh2 in vivo, we delivered an AAV vector encoding a gRNA expression cassette, Cre recombinase, under the control of the neuron-specific Syn1 promoter, and green fluorescent protein (GFP) to track transduced cells, by stereotactic injection into the dorsal hippocampus of dCas9p300 heterozygous mice (Fig. 2a and Supplementary Fig. 8a). For each mouse, one side of the brain was injected with a gRNA targeting Fos Enh2 and the other side was injected with a control non-targeting gRNA against LacZ as an in-animal control. Both sides of the hippocampus showed similar GFP expression, and immunofluorescence staining showed robust detection of Cas9 in neurons, confirming that the Cre virus was inducing conditional dCas9p300 expression (Supplementary Fig. 8b). We allowed one cohort of the mice to explore a set of novel objects in the open field, which is a stimulus that induces expression of Fos in the hippocampus¹⁴. As expected, immunostaining for FOS protein in the dentate gyrus region of the hippocampus showed very few cells expressing a high level of induced FOS. However, in each brain there was a significantly greater number of high FOS-positive cells on the side expressing the *Fos* Enh2-targeting gRNA than the side expressing the LacZ control gRNA (Fig. 2b,c). Importantly, quantification of FOS protein levels across all of the transduced cells showed that the distribution of FOS was significantly increased in the cells expressing the *Fos* Enh2-targeting gRNA compared with those expressing the LacZ-targeting gRNA (Supplementary Fig. 8c), consistent with dCas9p300-dependent regulation of *Fos* gene expression in a cell-autonomous manner.

A key application of transgenic dCas9p300 mice in the regulation of neuronal gene expression in vivo is the ability to determine the consequences of epigenome editing on the function of physiologically relevant neuronal circuits in the intact brain. To determine whether dCas9p300-driven increases in FOS protein levels were sufficient to change neuronal physiology, we cut acute slices of hippocampus from a second cohort of dCas9p300 mice and performed current-clamp recordings from virally transduced CA1 neurons (Supplementary Fig. 8d,e). Neurons expressing either the Fos Enh2 gRNA or the LacZ gRNA fired action potentials in response to progressive current steps (Fig. 2d). However, the action potential stimulus-response curves were significantly different between the two treatments. The maximum firing rate was reduced for the neurons expressing the Fos Enh2 gRNA compared with neurons expressing the LacZ control gRNA (Fig. 2e). However, the rheobase, that is, the lowest input current at which neurons begin to fire spikes, and the initial spike latency were both significantly reduced in neurons expressing the Fos Enh2 gRNA compared with the LacZ gRNA controls (Fig. 2f,g). These data indicate increased excitability of the Fos Enh2-edited neurons. Importantly, the input resistance and the membrane time constants were unchanged between the conditions (Fig. 2h,i). This suggests that the differences in action potential firing were due to changes in active, rather than passive, membrane properties. Taken together, these data show that dCas9p300-mediated epigenome editing of a single Fos enhancer in the adult brain in vivo induces changes in FOS protein levels that are sufficient to modulate neuronal physiology.

Targeted gene repression in the liver. For characterization of the dCas9^{KRAB} mice, we chose to target *Pcsk9* given that loss of PCSK9 protein is known to reduce serum levels of low-density lipoprotein (LDL) cholesterol⁴⁴. In a previous study, AAV co-delivery of the smaller dCas9 from *S. aureus* fused to the KRAB domain and a *Pcsk9*-targeted gRNA repressed *Pcsk9* in the liver, resulting in reduced serum LDL cholesterol levels²¹. We delivered AAV9

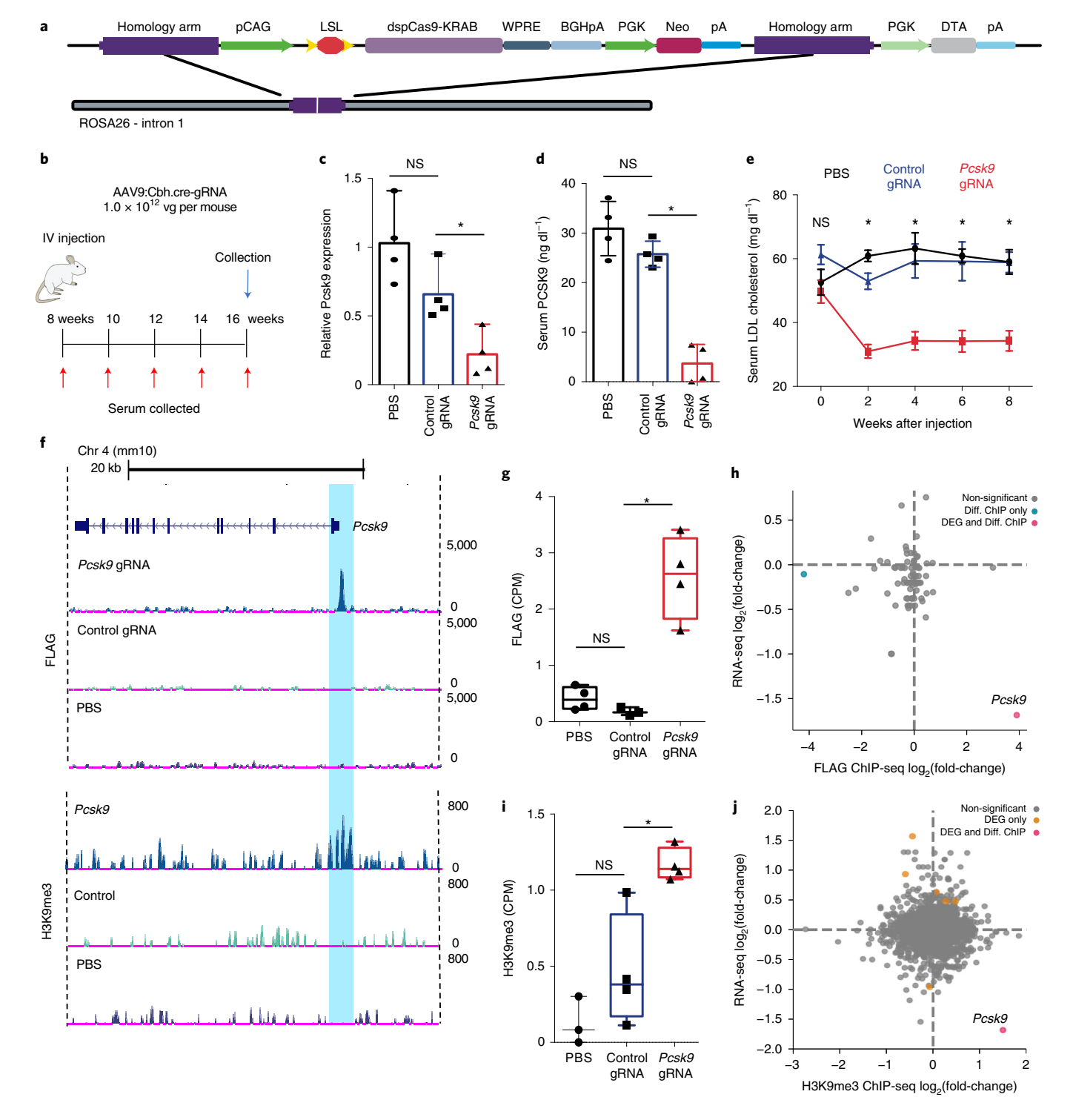
Fig. 3 | AAV-based gRNA and Cre recombinase delivery to Rosa26:LSL-dCas9KRAB mice represses Pcsk9 and catalyzes targeted histone methylation.

a, Schematic diagram of the dCas9^{KRAB} knock-in locus. b, Schematic diagram of the experiment to test *Pcsk9* repression in the dCas9^{KRAB} mice. c, *Pcsk9* mRNA quantification 8 weeks after injection in liver tissue lysates isolated from mice injected with PBS or AAV9 encoding Cre and either a control non-targeting or Pcsk9-targeting gRNA (n=4 per group, one-way ANOVA with Dunnett's post-hoc test, *P=0.0021). **d**, PCSK9 serum protein levels at 4 weeks after injection of PBS or AAV9 encoding Cre and either a control non-targeting or Pcsk9-targeting gRNA (n=4 per group, one-way ANOVA with Dunnett's post-hoc test, *P=0.0001). **e**, LDL cholesterol levels in the serum at 8 weeks after injection of PBS or AAV9:Cbh.Cre containing either a control non-targeting or Pcsk9-targeting gRNA (n=4 per group, two-way ANOVA with Tukey's post-hoc test, *P < 0.0001). **f**, Representative browser tracks of dCas9^{KRAB} (FLAG epitope) and H3K9me3 ChIP-Seq data from liver samples at 8 weeks after treatment (replicates are presented in Supplementary Figs. 10 and 11). The blue highlighted region corresponds to the area surrounding the gRNA target site in the Pcsk9 promoter. Chr-4 (mm10), chromosome 4 (Genome Reference Consortium Mouse Build 38). g, dCas9-FLAG ChIP-seq quantification of sequencing counts in the Pcsk9 promoter in samples treated with Pcsk9-targeted gRNA (n=4), control non-targeting gRNA (n=3) or PBS (n=4) (one-way ANOVA with Dunnett's post-hoc test, *P < 0.05). h, log₃(fold-change) of RNA-seq and FLAG ChIP-seq signal comparing read counts in peaks between samples treated with Pcsk9-targeted gRNA (n = 4) and control non-targeting gRNA (n=3), showing the relationship between gene expression and genome-wide dCas9^{KRAB} binding (FDR < 0.05). i, H3K9me3 ChIP-seq quantification of sequencing counts in the Pcsk9 promoter in samples treated with Pcsk9-targeted gRNA (n=4), control non-targeting gRNA (n=4) or PBS (n=4) (one-way ANOVA with Dunnett's post-hoc test, *P < 0.05.). \mathbf{j} , $\log_2(\text{fold-change})$ of RNA-seq and H3K9me3 ChIP-seq signal comparing read counts in peaks for samples treated with the Pcsk9-targeting gRNA (n=4) and the control non-targeting gRNA (n=4, FDR < 0.05). DEG, differentially expressed gene (orange dot); Diff. ChIP, differentially enriched ChIP-seq signal (blue dot); DEG and Diff. ChIP, differentially expressed gene and ChIP-seq enrichment (red dot). All bar-plot error bars represent standard deviation, and all boxplots are drawn from the 25th to the 75th percentile with the horizontal bar at the mean and the whiskers extending to the minima and maxima.

encoding Cre and an *S. pyogenes* gRNA targeting the same sequence in the *Pcsk9* promoter by tail vein injection to 8-week-old dCas9^{KRAB} mice (Fig. 3a), and compared them with control mice injected with saline or a corresponding vector containing a non-targeting control gRNA (Fig. 3b). At 8 weeks after injection, we collected the mouse livers and assessed the *Pcsk9* mRNA levels. We found that *Pcsk9* mRNA levels were reduced by ~70% when dCas9^{KRAB} was targeted to the promoter of *Pcsk9* compared with the non-targeting gRNA and saline controls (Fig. 3c). We also measured serum PCSK9 levels at 4 weeks after injection and found an ~90% reduction in samples treated with the *Pcsk9*-targeted gRNA as compared with the

controls (Fig. 3d). Additionally, serum was collected every 2 weeks during the 8 week experiment to assess LDL cholesterol levels (Fig. 3b). There was an ~45% reduction in serum LDL cholesterol levels at each time point from 2 to 8 weeks (Fig. 3e). Upon *Pcsk9* repression, LDL receptor protein levels increase due to lack of receptor degradation⁴⁵, which was confirmed by western blot in three of the four *Pcsk9*-targeted animals (Supplementary Fig. 9a).

To assess the specificity of gene regulation by dCas9^{KRAB} in these transgenic mice, we performed RNA-seq and ChIP-seq on liver tissue samples from dCas9^{KRAB} heterozygous mice injected with AAV encoding Cre and the *Pcsk9*-targeted gRNA, AAV encoding Cre and



the control non-targeting gRNA, or saline controls. For RNA-seq, we performed comparisons of treatment with the Pcsk9-targeted gRNA with both the control gRNA and the saline controls. In both cases, Pcsk9 was one of the most strongly downregulated genes, with only 15 and 6 other genes, respectively, that were significantly changed transcriptome-wide (Benjamini-Hochberg false discovery rate (FDR) < 0.01) (Supplementary Fig. 6d-f). ChIP-seq was performed using an anti-FLAG antibody for dCas9 binding specificity and a histone 3 lysine 9 trimethylation (H3K9me3) antibody to detect histone methylation as a result of dCas9KRAB-mediated recruitment of methyltransferases (Fig. 3f-j and Supplementary Figs. 10 and 11). Specific and significantly enriched dCas9 binding to the gRNA target site upstream of Pcsk9 was readily detected (Fig. 3f,g). Additionally, significant increases in H3K9me3 deposition in the target region of the Pcsk9-targeted gRNA were evident compared with the non-targeting control gRNA or saline controls (Fig. 3f,i). The dCas9KRAB binding was also highly specific genomewide, given that the Pcsk9 gRNA target site was one of only two significantly different peaks between samples treated with the Pcsk9 gRNA and the control gRNA in the dCas9 ChIP (Fig. 3h) and the only significantly different peak in the H3K9me3 ChIP (Fig. 3j).

Targeted gene activation and repression in primary immune cells. To further demonstrate the versatility of the dCas9^{p300} and dCas9^{KRAB} mice, we tested the modulation of expression of the master regulator transcription factor *Foxp3* in CD4⁺ T cells. *Foxp3* is essential for the development of a specialized arm of regulatory CD4⁺ T cells (T_{reg} cells) that plays a critical role in the attenuation and maintenance of the immune response to self and foreign pathogens^{46–49}. Activation of *Foxp3* expression and the generation of T_{reg} cells with immunosuppressive properties is of interest for cellular immunotherapies. Prior work has shown that lentiviral delivery of dCas9^{p300} targeted to the promoter of *Foxp3* is sufficient to increase FOXP3 protein levels⁵⁰.

We activated Foxp3 in T cells from the dCas9p300 mice using a Foxp3-enhanced (e)GFP, CD4-Cre, Rosa26-LSL-dCas9p300 cross to conditionally express dCas9p300 in all CD4+ T cells. Spleen and lymph nodes were isolated from these mice, dissociated, and CD4+/CD25-/ CD44lo/CD62Lhi-naive T (Tn) cells were purified by fluorescenceactivated cell sorting (FACS) (Supplementary Fig. 12a-c). Tn cells were cultured in T-cell antigen receptor-stimulating conditions (Th0) consisting of plate-bound α -CD3, α -CD28, the blocking antibodies α -interleukin (IL)-4 and α -interferon (IFN)- γ , and IL-2 prior to their transduction with retroviral supernatant containing a gRNA expression cassette. We first tested a panel of 12 gRNAs targeting the *Foxp3* promoter and identified four gRNAs immediately upstream of the TSS that had an activating effect (Supplementary Fig. 2b,d,e). We selected *Foxp3*-gRNA-5 and a non-targeting control gRNA for all downstream experiments. Following retroviral delivery of this Foxp3-targeting gRNA, Foxp3 activation was detected in ~30% of transduced cells as measured using the FOXP3-eGFP signal by flow cytometry (Fig. 4a,b). We verified the gene activation with RT-qPCR and found that the recruitment of dCas9^{p300} to the Foxp3 promoter led to an ~50-fold increase of Foxp3 expression relative to the control gRNA or untreated Th0 T cells (Fig. 4c). Using RNA-seq to assess gene expression in Foxp3 gRNA-treated Th0 cells, we found that relative to Th0 cells treated with the control gRNA, FoxP3 was the only differentially expressed gene in the genome (Fig. 4h and Supplementary Fig. 13).

To quantify changes in genome-wide histone acetylation made by dCas9^{p300}, we performed ChIP-seq for H3K27ac in Th0 cells from *Cd4-Cre*-positive, dCas9^{p300}-positive mice transduced with *Foxp3*-targeting or control gRNAs. We identified a significant enrichment in H3K27ac at the gRNA target site, and only 25 other H3K27ac peak regions were detected as differentially acetylated genome-wide (Fig. 4f-h and Supplementary Fig. 5b). Together, the

RNA-seq and ChIP-seq analyses highlight the specificity and efficacy of targeting dCas9p300 to one location of the genome (Fig. 4h). However, when we compared RNA-seq and ChIP-seq in Th0 cells treated with the Foxp3 gRNA from mice with or without Cd4-Cre, we observed numerous differences in gene expression and H3K27 acetylation (Supplementary Fig. 5h). When comparing RNA-seq data from Cre-negative and Cre-positive cells, the same set of genes was found to be differentially expressed regardless of whether the cells were treated with Foxp3-targeting or control gRNA, further supporting a gRNA-independent effect of active dCas9p300 expression on the baseline epigenetic state in this mouse strain (Supplementary Fig. 13). This effect is specific to the dCas9^{p300} mice and is not observed in dCas9KRAB mice when comparing liver samples from mice treated with either Pcsk9-targeting gRNA or saline (Supplementary Fig. 5f,i). These results illustrate the need for experimental controls that include an active dCas9^{p300} for comparisons with an accurate baseline epigenetic state.

To test the capacity of FOXP3-positive Th0 cells generated by targeted epigenome editing to function as $T_{\rm reg}$ cells, we used an in vitro suppression assay to test their ability to limit the proliferation of activated CD4+ T cells in co-culture. The cells treated with Foxp3-targeting gRNA showed enhanced suppression relative to untreated cells or cells treated with gRNA controls, and had a suppressive activity similar to that of the positive control induced (i) $T_{\rm reg}$ cells generated in vitro using established protocols (Fig. 4d,e). To verify that the suppression activity was mediated by the gRNA-treated cells, we performed a suppression assay using serial dilutions of the number of Foxp3-induced cells in co-culture and found a dose-dependent suppressive effect (Supplementary Fig. 12f,g).

To demonstrate gene repression in another cell type from the dCas9KRAB mice ex vivo, we isolated naive CD4+ T cells from the lymph nodes and spleen of Cd4:Cre/dCas9KRAB mice and generated FOXP3-positive iT_{reg} cells in vitro via T-cell antigen receptor activation and treatment with IL-2 and transforming growth factor (TGF)- β 1. The iT_{reg} cells were transduced with retrovirus containing either the Foxp3-targeting or non-targeting gRNAs. We achieved an ~70% reduction in Foxp3 mRNA levels in cells with dCas9KRAB targeted to the Foxp3 promoter as compared with untreated iT_{reg} cells or those treated with the control gRNA (Fig. 4i). In addition, we assessed FOXP3 protein levels by immunostaining and found a significant reduction in the percentage of FOXP3-positive cells when transduced with the Foxp3-targeting gRNA as compared with controls (Fig. 4j,k). These results confirm our ability to repress genes in multiple tissues and cell types of the dCas9KRAB mouse line both in vivo and ex vivo.

Discussion

Perturbation of gene expression has long been a powerful tool for uncovering the functions of genes. Recent technological advances have enabled not only the study of gene function, but also the mechanism by which the genes themselves are regulated. Using dCas9 fused to epigenome modifiers has proven to be a productive strategy to uncover unknown gene function, to map regions of the non-coding genome and to validate potential therapeutic applications using CRISPR-based epigenome editors in vivo. Here, we describe the generation and characterization of Cre-inducible dCas9p300 and dCas9KRAB transgenic mouse lines for targeted activation or repression of promoters and non-coding regulatory elements in vivo or in primary cells ex vivo, including in the liver, T cells, fibroblasts and neurons. We demonstrate induction of dCas9 epigenome editor expression using viral or transgenic Cre delivery combined with viral gRNA delivery. The targeted gene activation or repression induced changes in both mRNA transcript levels and protein changes that elicit downstream phenotypes. Concomitant with expression changes, we show targeted deposition of histone

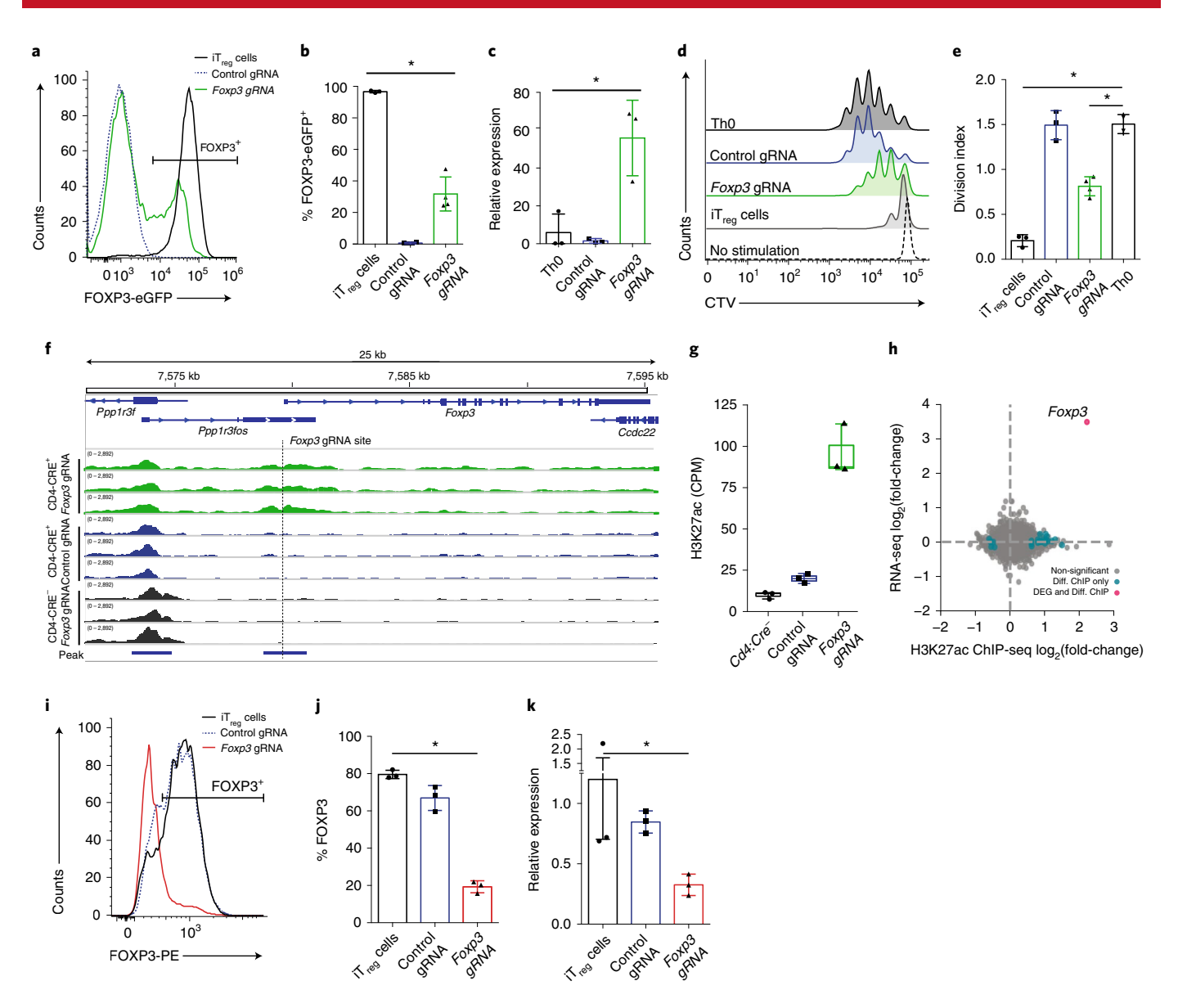


Fig. 4 | Epigenome editing in T cells for activation and repression of Foxp3. a, Flow cytometry analysis of FOXP3-eGFP expression in CD4+ T cells purified from dCas9⁹³⁰⁰;CD4:Cre;Foxp3:eGFP mice cultured in vitro under Th0 polarization conditions (IL-2) after transduction with retrovirus encoding either the Foxp3 gRNA or the control gRNA. Cells cultured in iT_{rep} cell polarization conditions (IL-2, TGF-β1) were included as a positive control for Foxp3 expression. **b**, The percentage of Thy1.1-positive cells that were FOXP3-EGFP positive (P < 0.0001; one-way ANOVA with Dunnett's post-hoc test; iT, ep cells, n = 3; control gRNA and Foxp3 gRNA, n=4). c, RT-qPCR measurement of Foxp3 mRNA levels in Th0 cells with no virus compared with cells treated with Foxp3-targeting gRNA or with control non-targeting gRNA (P = 0.0190, one-way ANOVA with Dunnett's post-hoc test, n = 3 per condition). **d**, Flow cytometry histograms showing proliferation of Cell Trace Violet (CTV)-labeled CD4+/FOXP3-eGFP- conventional T cells (Tconv) after 72h of in vitro co-culture with aCD3/ aCD28 dynabeads and either FOXP3-eGFP+ iT_{nex} cells (n=3), ThO cells (n=2), FACS-purified Thy1.1+/FOXP3-eGFP+ cells treated with Foxp3 gRNA (n=3) or Thy1.1+ cells treated with control non-targeting gRNA (n=3). Unstimulated T cells served as a no-activation control. **e**, Suppressive capacity of T_{ree} cells summarized as the division index of Tconv (P < 0.0001, one-way ANOVA with Tukey's post-hoc test). f, Browser track of H3K27ac ChIP-seq read counts at the Foxp3 locus in transduced ThO cells from a Cd4:Cre-positive or Cd4:Cre-negative Rosa26:LSL-dCas9e300 mouse. g, H3K27ac ChIP-seq read counts per million in the MACS2-called peak that intersects the Foxp3 gRNA target site for each genotype and gRNA treatment (Foxp3 gRNA-treated Cd4:Cre-positive ThO cells, control gRNA-treated Cd4:Cre-positive ThO cells, and Foxp3 gRNA-treated Cd4:Cre-negative ThO cells, n=3 per condition). **h**, Scatter plot showing log₂(fold-change) of gene expression and H3K27ac enrichment when comparing read counts from Cd4:Cre-positive Rosa26:LSL-dCas9^{a300} Th0 cells treated with Foxp3 gRNA to control gRNA (FDR < 0.01). DEG, differentially expressed gene (orange dot); Diff. ChIP, differentially enriched ChIP-seq signal (blue dot); DEG and Diff. ChIP, differentially expressed gene and ChIP-seq enrichment (red dot). i, Flow cytometry analysis of FOXP3 expression in CD4+ T cells purified from $dCas9^{KRAB}$ mice cultured in vitro under iT_{reg} cell polarization conditions and transduced with retrovirus encoding the indicated gRNAs. j, The percentage of Thy1.1-positive cells that were FOXP3-EGFP-positive for each gRNA treatment (P < 0.0001, one-way ANOVA with Dunnett's post-hoc test, n=3 per condition). **k**, RT-qPCR measurement of Foxp3 mRNA levels in iT_{res} cells treated with no virus, control gRNA or Foxp3-targeting gRNA (P < 0.0135, one-way ANOVA with Dunnett's post-hoc test, n = 3 per condition). All bar-plot error bars represent the standard deviation, and all boxplots are drawn from the 25th to 75th percentile with the horizontal bar at the mean and the whiskers extending to the minima and maxima.

marks subsequent to the recruitment of dCas9-based epigenetic effectors at both promoters and enhancers.

An unbiased, comprehensive, genome-wide analysis of epigenome editing specificity using ChIP-seq and RNA-seq showed both a high level of precision in DNA targeting and interesting differences between the dCas9^{p300} and dCas9^{KRAB} editors. The dCas9^{p300} editor was highly precise and robust when compared with a control non-targeting gRNA. However, when compared with cells in which dCas9p300 was not induced, there were widespread changes to H3K27ac and gene expression. Interestingly, these changes did not appear to result in any adverse phenotype. Given that the off-target changes were similar between the targeting and non-targeting gRNA in T cells, we interpret the changes to be gRNA independent and related to the expression of the constitutively active core catalytic domain of the p300 acetyltransferase that may alter the genome-wide epigenetic baseline of these cells. This is consistent with previous observations that dCas9 fused to catalytic enzymes such as DNA methyltransferases can exhibit gRNA-independent changes⁵¹, and underscores the importance of using proper gRNA controls to determine the consequences of modulating gene expression through epigenome editing. In contrast to dCas9p300, which has inherent non-specific catalytic activity, dCas9KRAB serves as a scaffold for the recruitment of other enzymatic histone modifiers. Accordingly, target changes to gene expression and epigenetic state were highly specific when compared with the non-targeting gRNA or saline controls, which was consistent with the high level of specificity of DNA targeting and histone modifications.

Following the development of CRISPR-Cas9 for genome editing in human cells⁵²⁻⁵⁶, a Cre-inducible Cas9 nuclease transgenic mouse was quickly generated and widely distributed for in vivo studies of gene function and the genetics of disease²⁸. This mouse line has been essential to numerous important breakthroughs including in vivo dissection of gene function⁵⁷ studies of gene regulatory networks⁵⁸, and in vivo genetic screens⁵⁹. We expect these new dCas9 epigenome editor transgenic mice to be similarly powerful for enabling in vivo studies of endogenous gene knockdown, activation and perturbation of epigenetic states. Accordingly, the mice have been deposited for distribution via The Jackson Laboratory (stock numbers 033065 (dCas9^{p300}) and 033066 (dCas9^{KRAB})).

Online content

Any methods, additional references, Nature Research reporting summaries, source data, extended data, supplementary information, acknowledgements, peer review information; details of author contributions and competing interests; and statements of data and code availability are available at https://doi.org/10.1038/s41592-021-01207-2.

Received: 17 May 2020; Accepted: 8 June 2021; Published online: 2 August 2021

References

- Thakore, P. I., Black, J. B., Hilton, I. B. & Gersbach, C. A. Editing the epigenome: technologies for programmable transcription and epigenetic modulation. *Nat. Methods* 13, 127–137 (2016).
- Gilbert, L. A. et al. CRISPR-mediated modular RNA-guided regulation of transcription in eukaryotes. Cell 154, 442–451 (2013).
- 3. Hilton, I. B. et al. Epigenome editing by a CRISPR-Cas9-based acetyltransferase activates genes from promoters and enhancers. *Nat. Biotechnol.* **33**, 510–517 (2015).
- Maeder, M. L. et al. CRISPR RNA-guided activation of endogenous human genes. Nat. Methods 10, 977–979 (2013).
- Perez-Pinera, P. et al. RNA-guided gene activation by CRISPR-Cas9-based transcription factors. Nat. Methods 10, 973–976 (2013).
- Chavez, A. et al. Highly efficient Cas9-mediated transcriptional programming. Nat. Methods 12, 326–328 (2015).
- Tanenbaum, M. E., Gilbert, L. A., Qi, L. S., Weissman, J. S. & Vale, R. D. A protein-tagging system for signal amplification in gene expression and fluorescence imaging. *Cell* 159, 635–646 (2014).

 Konermann, S. et al. Genome-scale transcriptional activation by an engineered CRISPR-Cas9 complex. *Nature* 517, 583–588 (2015).

- Liu, X. S. et al. Editing DNA methylation in the mammalian genome. *Cell* 167, 233–247 (2016).
- Stepper, P. et al. Efficient targeted DNA methylation with chimeric dCas9-Dnmt3a-Dnmt3L methyltransferase. Nucleic Acids Res. 45, 1703–1713 (2017).
- Yeo, N. C. et al. An enhanced CRISPR repressor for targeted mammalian gene regulation. *Nat. Methods* 15, 611–616 (2018).
- Thakore, P. I. et al. Highly specific epigenome editing by CRISPR-Cas9 repressors for silencing of distal regulatory elements. *Nat. Methods* 12, 1143–1149 (2015)
- Carpenter, M. D. et al. Nr4a1 suppresses cocaine-induced behavior via epigenetic regulation of homeostatic target genes. *Nat. Commun.* 11, 504 (2020).
- Chen, L. F. et al. Enhancer histone acetylation modulates transcriptional bursting dynamics of neuronal activity-inducible genes. *Cell Rep.* 26, 1174–1188 (2019).
- Frank, C. L. et al. Regulation of chromatin accessibility and Zic binding at enhancers in the developing cerebellum. Nat. Neurosci. 18, 647–656 (2015).
- Black, J. B. et al. Targeted epigenetic remodeling of endogenous loci by CRISPR/Cas9-based transcriptional activators directly converts fibroblasts to neuronal cells. Cell Stem Cell 19, 406–414 (2016).
- Liu, Y. et al. CRISPR activation screens systematically identify factors that drive neuronal fate and reprogramming. Cell Stem Cell 23, 758–771 (2018).
- 18. Weltner, J. et al. Human pluripotent reprogramming with CRISPR activators. *Nat. Commun.* **9**, 2643 (2018).
- Liu, P., Chen, M., Liu, Y., Qi, L. S. & Ding, S. CRISPR-based chromatin remodeling of the endogenous Oct4 or Sox2 locus enables reprogramming to pluripotency. *Cell Stem Cell* 22, 252–261 (2018).
- Chakraborty, S. et al. A CRISPR/Cas9-based system for reprogramming cell lineage specification. Stem Cell Rep. 3, 940–947 (2014).
- Thakore, P. I. et al. RNA-guided transcriptional silencing in vivo with S. aureus CRISPR-Cas9 repressors. Nat. Commun. 9, 1674 (2018).
- Matharu, N. et al. CRISPR-mediated activation of a promoter or enhancer rescues obesity caused by haploinsufficiency. Science 363, eaau0629 (2019).
- Klann, T. S. et al. CRISPR-Cas9 epigenome editing enables high-throughput screening for functional regulatory elements in the human genome. *Nat. Biotechnol.* 35, 561–568 (2017).
- Fulco, C. P. et al. Systematic mapping of functional enhancer-promoter connections with CRISPR interference. Science 354, 769–773 (2016).
- Fulco, C. P. et al. Activity-by-contact model of enhancer-promoter regulation from thousands of CRISPR perturbations. Nat. Genet. 51, 1664–1669 (2019).
- Simeonov, D. R. et al. Discovery of stimulation-responsive immune enhancers with CRISPR activation. *Nature* 549, 111–115 (2017).
- Ran, F. A. et al. In vivo genome editing using Staphylococcus aureus Cas9. Nature 520, 186–191 (2015).
- Platt, R. J. et al. CRISPR-Cas9 knockin mice for genome editing and cancer modeling. Cell 159, 440–455 (2014).
- Liao, H. K. et al. In vivo target gene activation via CRISPR/Cas9-mediated trans-epigenetic modulation. Cell 171, 1495–1507 (2017).
- Zhou, H. et al. In vivo simultaneous transcriptional activation of multiple genes in the brain using CRISPR-dCas9-activator transgenic mice. Nat. Neurosci. 21, 440–446 (2018).
- Wangensteen, K. J. et al. Combinatorial genetics in liver repopulation and carcinogenesis with an in vivo CRISPR activation platform. *Hepatology* 68, 663–676 (2018).
- Li, K. et al. Interrogation of enhancer function by enhancer-targeting CRISPR epigenetic editing. Nat. Commun. 11, 485 (2020).
- Chew, W. L. et al. A multifunctional AAV-CRISPR-Cas9 and its host response. Nat. Methods 13, 868–874 (2016).
- Nelson, C. E. et al. Long-term evaluation of AAV-CRISPR genome editing for Duchenne muscular dystrophy. Nat. Med. 25, 427–432 (2019).
- Li, A. et al. AAV-CRISPR gene editing is negated by pre-existing immunity to Cas. Mol. Ther. 28, 1432–1441 (2020).
- Moreno, A. M. et al. Immune-orthogonal orthologues of AAV capsids and of Cas9 circumvent the immune response to the administration of gene therapy. Nat. Biomed. Eng. 3, 806–816 (2019).
- Ferdosi, S. R. et al. Multifunctional CRISPR-Cas9 with engineered immunosilenced human T cell epitopes. Nat. Commun. 10, 1842 (2019).
- Ferber, S. et al. Pancreatic and duodenal homeobox gene 1 induces expression of insulin genes in liver and ameliorates streptozotocin-induced hyperglycemia. *Nat. Med.* 6, 568–572 (2000).
- Tang, D. Q. et al. Reprogramming liver-stem WB cells into functional insulin-producing cells by persistent expression of Pdx1- and Pdx1-VP16 mediated by lentiviral vectors. *Lab. Invest.* 86, 83–93 (2006).
- Chen, T. et al. Chemically controlled epigenome editing through an inducible dCas9 system. J. Am. Chem. Soc. 139, 11337–11340 (2017).
- 41. Chen, X. et al. A novel enhancer regulates MGMT expression and promotes temozolomide resistance in glioblastoma. *Nat. Commun.* **9**, 2949 (2018).

- 42. Wang, A. S. et al. The histone chaperone FACT induces Cas9 multi-turnover behavior and modifies genome manipulation in human cells. *Mol. Cell* **79**, 221–233 (2020).
- Guo, L. et al. A combination strategy targeting enhancer plasticity exerts synergistic lethality against BETi-resistant leukemia cells. *Nat. Commun.* 11, 740 (2020).
- 44. Abifadel, M. et al. Mutations in PCSK9 cause autosomal dominant hypercholesterolemia. *Nat. Genet.* **34**, 154–156 (2003).
- 45. Zhang, D. W. et al. Binding of proprotein convertase subtilisin/kexin type 9 to epidermal growth factor-like repeat A of low density lipoprotein receptor decreases receptor recycling and increases degradation. *J. Biol. Chem.* 282, 18602–18612 (2007).
- Brunkow, M. E. et al. Disruption of a new forkhead/winged-helix protein, scurfin, results in the fatal lymphoproliferative disorder of the scurfy mouse. *Nat. Genet.* 27, 68–73 (2001).
- Fontenot, J. D., Gavin, M. A. & Rudensky, A. Y. Foxp3 programs the development and function of CD4+ CD25+ regulatory T cells. *Nat. Immunol.* 4, 330–336 (2003).
- Hori, S., Nomura, T. & Sakaguchi, S. Control of regulatory T cell development by the transcription factor Foxp3. Science 299, 1057–1061 (2003).
- Khattri, R., Cox, T., Yasayko, S. A. & Ramsdell, F. An essential role for Scurfin in CD4+ CD25+ T regulatory cells. *Nat. Immunol.* 4, 337–342 (2003).
- Okada, M., Kanamori, M., Someya, K., Nakatsukasa, H. & Yoshimura, A. Stabilization of Foxp3 expression by CRISPR-dCas9-based epigenome editing in mouse primary T cells. *Epigenetics Chromatin* 10, 24 (2017).

- Galonska, C. et al. Genome-wide tracking of dCas9-methyltransferase footprints. Nat. Commun. 9, 597 (2018).
- Jinek, M. et al. RNA-programmed genome editing in human cells. Elife 2, e00471 (2013).
- 53. Jinek, M. et al. A programmable dual-RNA-guided DNA endonuclease in adaptive bacterial immunity. *Science* 337, 816–821 (2012).
- Mali, P. et al. RNA-guided human genome engineering via Cas9. Science 339, 823–826 (2013).
- Cong, L. et al. Multiplex genome engineering using CRISPR/Cas systems. Science 339, 819–823 (2013).
- Cho, S. W., Kim, S., Kim, J. M. & Kim, J. S. Targeted genome engineering in human cells with the Cas9 RNA-guided endonuclease. *Nat. Biotechnol.* 31, 230–232 (2013).
- Swiech, L. et al. In vivo interrogation of gene function in the mammalian brain using CRISPR-Cas9. *Nat. Biotechnol.* 33, 102–106 (2015).
- Parnas, O. et al. A genome-wide CRISPR screen in primary immune cells to dissect regulatory networks. Cell 162, 675–686 (2015).
- Chen, S. et al. Genome-wide CRISPR screen in a mouse model of tumor growth and metastasis. Cell 160, 1246–1260 (2015).

Publisher's note Springer Nature remains neutral with regard to jurisdictional claims in published maps and institutional affiliations.

© The Author(s), under exclusive licence to Springer Nature America, Inc. 2021

Methods

Generation of Rosa26:LSL-dCas9-p300 and Rosa26:LSL-dCas9-KRAB transgenic lines. All experiments involving animals were conducted with strict adherence to the guidelines for the care and use of laboratory animals of the National Institutes of Health. All experiments were approved by the Institutional Animal Care and Use Committee at Duke University.

To generate mouse lines for conditional expression of these dCas9 fusion proteins, we used a modified pAi9 targeting vector. The pAi9 vector targets the Rosa26 locus and contains the 5' Rosa homology arm, a CAG promoter, a loxP-flanked triple polyadenylation (pA) signal stop cassette (LSL), a codon-optimized dCas9-p300 cassette3 or dCas9-KRAB (ref. 12) with either a 1X-FLAG or 3X-FLAG, respectively, a woodchuck hepatitis post-transcriptional regulatory element (WPRE), a bovine growth hormone pA, a phosphoglycerate kinase (PGK)-Neo-pA selection cassette, and the 3' homology arm. This modified pAi9 targeting vector was electroporated into hybrid G4 B6N/129S6 ES cells, and targeting of the ROSA locus was confirmed on PCR and sequencing. Positive clones were expanded and injected into the 8-cell morulae of ICR mice. Chimeric mice were then mated to establish the transgenic line. The mice are genotyped using a forward primer, GCAGCCTCTGTTCCACATACAC, a reverse primer, TAAGCCTGCCCAGAAGACTC, and a second F primer, AAAGTCGCTCTGAGTTGTTAT. The PCR conditions used for genotyping are 95 °C for 5 min, followed by 35 cycles of 95 °C for 30 s, 57 °C for 45 s, 72 °C for 1 min and 72 °C for 3 min, with a 12 °C hold. The expected product size for the WT band is 235 bp, and that for the knock-in is 162 bp. All mice used in the experiments were dCas9^{p300} or dCas9^{KRAB} heterozygous animals.

The new mouse lines are available from The Jackson Laboratory, with the stock numbers of 033065 for Rosa26-LSL-dCas9-p300 and 033066 for Rosa26-LSL-dCas9-KRAB.

All mice were housed in pathogen-free barrier conditions with the exception of those mice used for stereotaxic injections. The mice were kept in ventilated racks at a temperature of $22\,^{\circ}\text{C} \pm 1\,^{\circ}\text{C}$ and a humidity of 30–70%, with food and water ad libitum. The mice used for the liver- and brain-targeting experiments had a 12–12 h light-dark cycle, whereas the mice used for T-cell experiments had a 14–10 h light-dark cycle. All mice were between 8 and 12 weeks old and were not selected based on sex, with the exception of those adult male mice used only for sterotaxic injection experiments.

Isolation and culture of primary dCas9^{p300} cells. Fibroblasts were isolated from the gastrocnemius and tibialis anterior of the hind limbs of 6-week-old dCas9^{p300} heterozygous animals using a modified version of a protocol by Springer et al.⁶⁰. Instead of proceeding with myoblast isolation, fibroblasts were isolated through selective trypsinization of the myoblasts out of the culture using 0.25% trypsin. Fibroblasts were then grown in DMEM supplemented with 10% fetal bovine serum (FBS).

The CGNs from male and female postnatal d7 dCas9p300 heterozygous pups were cultured following our published protocols¹⁵. In brief, the cerebellar cortex was removed and dissociated with papain, the granule neuron progenitors were purified by centrifugation through a Percoll gradient, and neurons were plated on poly-p-lysine-coated plates in neurobasal media with B27 supplements (Invitrogen), 1% FBS and penicillin-streptomycin. On d1 of in vitro culture, neurons were transduced with lentiviruses. All neurons received either two gRNAs targeting the Grin2c promoter (site 2-2 and site 2-3 from Frank et al. 15) or a control non-targeting gRNA complementary to a sequence in the LacZ gene¹⁴. The gRNAs were delivered in an FUGW-based U6 chimeric gRNA expression vector co-expressing GFP. In addition to the gRNA virus, one set of cells received a lentivirus expressing the Cre recombinase under the control of the hSyn1 promoter (Addgene 86641). This induced expression of the dCas9^{p300} transgene in the neurons. Other neurons received lentivirus expressing dCas9VP64 with the gRNAs to compare the functions of the two transgenes in neurons from the same cultures⁵. Viruses were titered on HEK293T cells before use and delivered at a multiplicity of

AAV cloning and production. An AAV backbone containing a gRNA cloning site, pCBh.Cre-WPRE-hGHpA, was obtained from Addgene (plasmid no. 60229). Two oligonucleotides per gRNA were purchased, annealed and cloned into the SapI cloning site. Prior to AAV production, inverted terminal repeats were verified by Smal digest. pCre-Pdx1.gRNA and pCre-control.gRNA were used to generate high-titer AAV9. Viral supernatants at the indicated titers were dialyzed with 350 mM NaCl and 5% D-sorbitol in PBS. For neurons, gRNAs for LacZ or Fos Enh2 sequences were cloned in the Sap1 site of an AAV backbone (Addgene no. 60231) with hSyn-Cre-2A-GFP. High-titer AAVs for intracranial delivery were produced in serotype AAV2/1 by the Duke University Viral Vector Core Facility.

Lentiviral cloning and production. Lentivirus production was carried out using standard procedures in HEK293T (ATCC CRL-11268) cells with the second-generation lentiviral vectors VSVg and ds.9 (ref. 61). Lentiviral preparations for fibroblast transduction were purified using Lenti-XTM (Clonetech, cat. no. 631232) to a 20X concentration. Fibroblasts were transduced at 1X concentration in the absence of polybrene for 24 h, media was then changed and fibroblasts

were returned to the growth media. For neurons, viruses were purified by ultracentrifugation and resuspended at a titer of $\sim\!5\times10^5$ infectious particles per µl PBS. Neurons were transduced in a solution of DMEM+0.5 µg ml $^{-1}$ polybrene for 6 h, then neurons were washed and returned to the conditioned medium for 5 d to allow for viral gene expression.

Retroviral cloning and production. Retrovirus was produced in PLAT-E cells (provided by Dan Littman) following standard procedures⁶². In brief, individual gRNA was cloned into the BbsI site of a Mouse Stem Cell Virus (MSCV) backbone that contained a gRNA expression cassette controlled by the mU6 promoter and a Thy1.1 reporter controlled by an hPGK promoter. Cloned vectors were transfected into PLAT-E cells using Lipofectamine 3000 (Thermo Fisher, cat. no. L3000008) and culture media was replaced after 16 h. Virus-containing media was collected 48 h or 72 h after transfection, spun at 800 ×g for 10 min and the viral supernatant was snap frozen in liquid nitrogen until the transduction of T cells. All sequences for gRNA protospacers can be found in Supplementary Table 1.

RNA isolation and RT-qPCR. RNA was isolated from fibroblasts using a Qiagen RNeasy Kit (cat. no. 74136). cDNA synthesis was performed using Superscript III with Vilo buffer. For Pdx1 quantification, the Taqman probes Mm00435565_m1 (for Pdx1, cat. no. 4453320) and Mm99999915_g1 (for Gapdh, cat. no. 4448489) were used along with Perfecta qPCR Fastmix II (cat. no. 95118-012). For Pcsk9 quantification, primers and conditions were used as described previously²¹ Neurons were collected for RNA extraction (using the Qiagen RNeasy Kit with on-column DNAse treatment), and oligo(dT) and random primers were primed for cDNA synthesis with the iScript cDNA Synthesis Kit (BioRad, cat. no. 1708891), and run for SYBR qPCR on a Quantstudio 3 real-time PCR system (Thermo Fisher). All gene expression values were normalized to Gapdh in the same well to control for sample handling. Sequences for qPCR primers can be found in Supplementary Table 1. T cells were collected using the Cells-to-CT 2-Step Taqman Kit (Thermo Fisher, cat. no. A35377) following the manufacturer's instructions. Foxp3 quantification was performed using the Taqman probes Mm00475162_m1 (for Foxp3, cat. no. 4331182) and Mm99999915_g1 (for Gapdh, cat. no. 4448489).

RNA-seq and differential expression analysis. For liver tissue, the RNA was isolated using the Qiagen RNeasy Plus Universal Kit (cat. no. 73404). RNA-seq was performed after poly(A)-tail enrichment and ribosomal RNA depletion of the RNA, and preparation of the libraries with an NEBNext Ultra II Kit (E7645L). For T cells, transduced cells were FACS purified using an SH800 cell sorter and a fluorescent antibody targeting Thy1.1. Cell pellets were processed using a Qiagen RNeasy RNA Extraction Kit. RNA-seq libraries were built from rRNA-depleted mRNA using the Illumina TruSeq mRNA Library Prep Kit (cat. no. 20020595). All RNA-seq samples were first validated for consistent quality using FastQC v0.11.2 (Babraham Institute). Raw reads were trimmed to remove adapters and bases with an average quality score (Phred33 score) of < 20 using a 4 bp sliding window (SLIDINGWINDOW:4:20) with Trimmomatic v0.32 (ref. 63). Trimmed reads were subsequently aligned to the primary assembly of the GRCm38 mouse genome using STAR v2.4.1a (ref. 64), removing alignments containing non-canonical splice junctions (-outFilterIntronMotifs RemoveNoncanonical). Aligned reads were assigned to genes in the GENCODE vM13 comprehensive gene annotation65 using the featureCounts command in the subread package with default settings (v1.4.6-p4, ref. 66). Differential expression analysis was performed using DESeq2 (v1.22.0, ref. 67) running on R (v3.5.1). In brief, raw counts were imported and filtered to remove genes with low or no expression, and to retain genes with 2 or more counts per million in two or more samples. Filtered counts were then normalized using the DESeq function, which uses estimated size factors to account for library size as well as gene and global dispersion. To find significant differentially expressed genes, nbinomWaldTest was used to test the coefficients in the fitted negative binomial generalized linear model (GLM) using the previously calculated size factors and dispersion estimates. Genes with a Benjamini-Hochberg FDR < 0.05 were considered significant (unless otherwise indicated). log2(fold-change) values were shrunk towards zero using the adaptive shrinkage estimator from the ashr R package⁶⁸. log₂(fold-change) was calculated using the ratio of read counts of samples treated with the Pdx1-targeted gRNA relative to control non-targeting gRNA in dCas9p300 cells. To estimate transcript abundance, transcripts per million were computed using the rsem-calculate-expression function in the RSEM v1.2.21 package69. Data were visualized using the pandas v0.23.3 and seaborn v0.9.0 packages in Python 2.7.11.

Protein isolation and western blot. Protein from tissue was isolated using Biomasher II mortar and pestle tubes in conjunction with RIPA or TGH buffer. Protein was quantified using a BCA assay. Novex NuPage 4–12% Bis-Tris gels were run for 45 min in MES running buffer and transferred onto nitrocellulose membranes for 1 h at 4°C in Towbin buffer with 20% MeOH. Membranes were blocked for non-specific binding overnight in 5% milk in Tris-buffered saline–Tween-20 (TBS-T). Primary antibodies were incubated in 5% milk in TBS-T either at room temperature for 2–3 h (Anti-Cas9, EnCor Biotechnology, cat. no. MCA-3F, 1:2,000) or overnight at 4°C (Anti-Gapdh, Cell Signaling, cat. no. 2118 L, 1:5,000; Anti-LDLR, Abcam, cat. no. ab52818, 1:1,000; anti-Actin, EMD Millipore,

cat. no. MAB1501, 1:5,000). After washing, secondary antibodies (Anti-rabbit HRP, Sigma, cat. no. A6154, 1:5,000; Anti-Mouse HRP, Santa Cruz, cat. no. sc-2005, 1:5,000) were incubated in 3% BSA in TBS-T. Membranes were visualized using Clarity western ECL substrate (cat. no. 1705061) from BioRad and imaged using a BioRad ChemiDoc XRS+. For neurons, cells were lysed directly in 1X RIPA buffer and blots were incubated with goat anti-mouse 680 (Biotium, cat. no. 20253, 1:5,000). Fluorescent immunoreactivity was imaged on a LICOR Odyssey and analyzed with LiCor Image Studio v4.0.

Stereotaxic injection of gRNA AAVs in mouse hippocampus. AAV:Syn1-Cre. gRNA containing a gRNA targeting either LacZ (control) or Fos Enh2 (experimental treatment) was stereotaxically injected into each hemisphere of the dorsal hippocampus of adult male $dCas9^{p:300}$ heterozygous mice such that each mouse had one control side and one experimental side (stereotaxic coordinates: anterior–posterior (AP), -2.3; medial–lateral (ML), +/-1.8; dorsal–ventral (DV), -1.8). Three weeks following transduction, mice were used for evaluation of Fos expression (n=3 mice) or for electrophysiology (n=2 mice). Virally expressed GFP was used to identify CA1 neurons for recording.

Histological staining. For PDX1 staining, livers were fixed overnight with 4% paraformaldehyde, and 12- μ m-thick cryostat sections were processed for immunofluorescence. Slides were washed in PBS and boiled in citrate buffer (10 mM citric acid, 0.05% Tween-20, pH 6.0) for 25 min at 95 °C, and were then kept for 20 min at room temperature (antigen retrieval). Slides were permeabilized with PBS containing 0.2% Triton for 20 min, washed with PBS and blocked with 3% BSA+0.1% Tween in PBS for 1 h. The primary antibody (Anti-PDX1-Antibody, Abcam, cat. no. ab47267, 1:100) was incubated overnight at 4 °C in blocking reagent. Sections were then washed and incubated with a specific secondary antibody coupled to Alexa Fluor 488 (Goat anti-Rabbit IgG, Life Technologies, cat. no. A27034, 1:200) and 4,6-diamidino-2-phenylindole. Confocal images were acquired with a Zeiss LSM 880 microscope.

For Fos staining in hippocampal sections, after 3 weeks following viral injection the mice were placed in an open field and allowed to explore three novel objects for a period of 2h. Mice were then perfused with 4% paraformaldehyde and the brains were coronally sectioned on a freezing microtome for immunostaining. The primary antibodies used were rabbit anti-c-Fos (Calbiochem, cat. no. PC38, 1:1,000) or rabbit anti-Cas9 (EnCor Biotechnology, cat. no. RPCA-CAS9-Sp, 1:1,000). These were detected using anti-rabbit Cy3 (1:500). Z-stack images through the dentate gyrus were obtained using a Leica SP8 upright confocal with a ×40 objective plus additional digital zoom. For each animal, the hemisphere infected with gRNA targeting Fos Enh2 was compared with the control hemisphere expressing the control LacZ gRNA. To count high Fos-expressing cells, z-stacks were converted to sum projections and thresholded using ImageJ. These counts were compared using a paired t-test. To determine whether there were changes in Fos intensity across the population of GFP-positive cells, regions of interest (ROIs) were created for each GFP-positive cell in a given region while blind to Fos expression. The fluorescence intensity of the Fos channel was then measured for each of these cells, to create a distribution of Fos intensities. The Fos signal for each cell was normalized to the average control hemisphere Fos value for a given animal. The resulting distributions were then compared using a Kolmogorov-Smirnoff test.

ChIP-seq and analysis. Livers were pulverized and fixed as described by Savic et al.70. Following fixation, livers were rocked at 4°C in 10 ml Farnham Lysis Buffer for 10 min, followed by centrifugation. Pellets were resuspended in 4 ml RIPA buffer, after which 1 ml RIPA containing resuspended liver was placed into a 15 ml tube with 800 mg Diagenode sonication beads (Diagenode, C01020031). This tube was sonicated for 30 cycles of 30 s on and 30 s off using a Bioruptor Pico (Diagenode) at 4°C. For CD4+ T cells, 2 million cells were fixed with 1% paraformaldehyde at room temperature for 10 min, quenched with 0.125 M glycine and washed twice with PBS. Fixed cells were lysed with 1 ml Farnhyme Lysis Buffer for 5 min on ice followed by centrifugation at 800 ×g for 5 min at 4 °C. Cell pellets were snap frozen before being resuspended in $100\,\mu \bar{l}$ RIPA buffer. Cells were then sonicated for 10 cycles of 30 s on and 30 s off using a Bioruptor Pico as previously mentioned. ChIP for all samples was performed using 5 µg of either Cas9 (Diagenode, cat. no. C15200229-100), Flag-M2 (Sigma, cat. no. F1804), H3K27ac (Abcam, cat. no. ab4729) or H3K9me3 (Abcam, cat. no. ab8898) antibodies. Following ChIP, ChIP-seq libraries were prepared using a Kapa HyperPrep Kit (Roche, cat. no. 07962312001) and sequenced using 50 bp single-end reads on an Illumina HiSeq4000 or 25 bp paired-end reads on an Illumina NextSeq 500. For analysis, adapter sequences were removed from the raw reads using Trimmomatic v0.32 (ref. 63). Reads were aligned to the primary assembly of the GRCm38 mouse genome using Bowtie v1.0.0 (ref. 71), reporting the best alignment with up to 2 mismatches (parameters -best -strata -v 2). Duplicates were marked using Picard MarkDuplicates v1.130 (http://broadinstitute.github.io/picard/), while low-mappability or blacklisted regions identified by the ENCODE project were filtered out from the final BAM files. Signal files were generated with deepTools bamCoverage (v3.0.1, ref. 72) ignoring duplicates, extending reads to 200 bp and applying reads per kilobase per million mapped reads (RPKM) normalization. Using the sequenced input controls, binding regions were identified using the

callpeak function in MACS2 v2.1.1.20160309 (ref. ⁷³). All MACS2 peaks were annotated with the TSS of the nearest gene using Gencode vM19 basic annotation data. For the differential binding analysis, first, a union peak set was computed by merging individual peak calls using BEDtools2 v2.25.0 (ref. ⁷⁴). Then, reads in peaks were estimated using featureCounts from the subread package v1.4.6-p4 (ref. ⁶⁶). The difference in binding was assessed with DESeq2 v1.22.0 (ref. ⁶⁷) using nbinomWaldTest to test coefficients in the fitted negative binomial GLM. Data were visualized using the pandas v0.23.3 and seaborn v0.9.0 packages in Python 2.7.11 or R v3.5.1.

ChIP-qPCR and analysis. For CGNs, chromatin immunoprecipitation was performed following the protocol of EZ-ChIP (Millipore, cat. no. 17-371). In brief, cells were lysed using SDS Lysis Buffer and sonicated for 1.5 h (Diagenode Bioruptor) at 4°C on the high setting with a 30 s on-off cycle. A total of 20 µl Dynabeads Protein G (Thermo Fisher, cat. no. 10003D) was pre-incubated with 2 μg antibodies in 1X PBS buffer for 4-6 h at 4 °C. Mouse anti-Cas9 antibodies (Encor, cat. no. MCA-3F9 and Diagenode, cat. no. C15200229-100) were used. Cell lysates were then incubated overnight with antibody-bead complexes at 4°C. Subsequently, the beads were washed with Low Salt Immune Complex Wash Buffer, High Salt Immune Complex Wash Buffer, LiCl Immune Complex Wash Buffer, and TE Buffer. Bound protein-DNA complexes were eluted with ChIP elution buffer and then the cross-links were reversed. Samples were treated with RNase A and Proteinase K for post-immunoprecipitation and then the DNA was purified using the QIAquick PCR Purification Kit (Qiagen, cat. no. 28104). The ChIP primer sequences are listed in Supplementary Table 1. ChIP for Grin2c was normalized to ChIP for Gapdh in the same sample to control for concentration and

Hippocampal slice electrophysiological recordings. Three weeks after viral injections into dCas9p300 heterozygous mice, the mice were anesthetized with isofluorane and transcardially perfused with ice-cold N-methyl-D-glucamine (NMDG) artificial cerebrospinal fluid (NMDG-ACSF, containing 92 mM NMDG, 2.5 mM KCl, 1.2 mM NaH₂PO₄, 30 mM NaHCO₃, 20 mM HEPES, 2 mM glucose, 5 mM sodium ascorbate, 2 mM thiourea, 3 mM sodium pyruvate, 10 mM MgSO₄, 0.5 mM CaCl₂) that was bubbled with 5% CO₂-95% O₂. The brain was extracted and sectioned into 300-µm-thick sagittal slices using a vibratome (VT-1000S, Leica Microsystems) in ice-cold oxygenated NMDG-ACSF. Coronal sections including the dorsal hippocampus were bubbled in the same solution at 37 °C for 8 min and transferred to oxygenated modified-HEPES ACSF at room temperature (20-25°C; 92 mM NaCl, 2.5 mM KCl, 1.2 mM NaH₂PO₄, 30 mM NaHCO₃, 20 mM HEPES, 2 mM glucose, 5 mM sodium ascorbate, 2 mM thiourea, 3 mM sodium pyruvate, $2\,\mathrm{mM}$ MgSO₄, $2\,\mathrm{mM}$ CaCl₂) for at least 1 h before recording. Recordings were performed in a submerged chamber, superfused with continuously bubbled ACSF (125 mM NaCl, 2.5 mM KCl, 1.25 mM NaH₂PO₄, 25 mM NaHCO₃, 25 mM glucose, 2 mM CaCl₂, 1 mM MgCl₂, 2 mM sodium pyruvate) at near-physiological temperature (34 ± 1 °C). For whole-cell current-clamp recordings, the electrodes (4–6 $M\Omega$) were filled with an intracellular solution containing 130 mM K-methylsulfonate, 5 mM NaCl, 10 mM HEPES, 15 mM EGTA, 12 mM phosphocreatine, 3 mM Mg-ATP, 0.2 mM Mg-GTP, 0.05 mM Alexa Fluor 594 cadaverine and 1% biotin. Current-clamp responses were recorded with a Multiclamp 700B amplifier (filtered at 2-4 kHz) and digitized at 10 kHz (Digidata 1440). Series resistance was always <20 M Ω and was compensated at 80–95%. Virally transduced pyramidal cells expressing GFP were visualized using infrared differential interference contrast and fluorescence video microscopy (Olympus; CoolLED) with a ×40 objective. Data were collected and analyzed off-line using the AxographX v1.7.6 and Neuromatic v3.0 packages (Think Random) in Igor Pro 6.22 A (WaveMetrics). The resting membrane potential was measured while cells were held at 0 pA. The action potential frequency was measured during holding currents of 0-500 pA. Rheobase was measured as the smallest current needed to depolarize the cell membrane. Initial spike latency was defined as the time from the onset of holding current change to the first measurable deflection of the potential from baseline. The membrane time constant was defined as the time it took the voltage level of the cell to decay to a resting state after delivering a 200 ms step of $-150 \,\mathrm{pA}$. Input resistance was measured using $\Delta V/\mathrm{pA} = \mathrm{m}\Omega$ for each current step and averaging across all current steps for individual neurons. All measurements were averaged across neurons. Finally, recorded neurons were labeled with biotin delivered through the patch pipette, and post-hoc confocal imaging of fixed slices confirmed GFP expression in the recorded neurons.

Novel object exploration and hippocampal expression of Fos. AAV vectors containing GFP and gRNA targeting either LacZ (control) or Fos Enh2 were injected into either hemisphere of the dorsal hippocampus of adult male dCas9^{p300} mice such that each mouse had one control hemisphere and one experimental hemisphere (stereotaxic coordinates AP, -2.3; ML, +/-1.8; DV, -1.8). Three weeks following AAV injection, mice were placed in an open field and allowed to explore three novel objects for a period of 2 h. Mice were then perfused with 4% paraformaldehyde and the brains were coronally sectioned on a freezing microtome for immunostaining. The primary antibodies used were rabbit anti-c-Fos (CalBiochem, cat. no. PC38, 1:1,000) and rabbit anti-Cas9 (EnCor

Biotechnology, cat. no. RPCA-CAS9-Sp, 1:1,000). These were detected using anti-rabbit Cy3 (1:500). Z-stack images through the dentate gyrus were obtained using a Leica SP8 upright confocal with a \times 40 objective plus additional digital zoom. For each animal, the hemisphere infected with gRNA targeting Fos Enh2 was compared with the control hemisphere expressing the control LacZ gRNA. To count high Fos-expressing cells, z-stacks were converted to sum projections and thresholded using ImageJ v1.46j (National Institutes of Health). These counts were compared using a paired t-test. To determine whether there were changes in Fos intensity across the population of GFP-positive cells, ROIs were created for each GFP-positive cell in a given region while blind to Fos expression. The fluorescence intensity of the Fos channel was then measured for each of these cells, to create a distribution of Fos intensities. The Fos signal for each cell was normalized to the average control hemisphere Fos value for a given animal. The resulting distributions were then compared using a Kolmogorov–Smirnoff test.

Purification of CD4 T cells for in vitro cultures. Rosa26-LSL-dCas9-p300 or Rosa26-LSL-dCas9-KRAB mice were backcrossed with a B6-Foxp3-eGFP mouse line (Jax stock no. 006772)^{75,76} for six generations and then crossed with the B6-CD4:Cre mouse line (Jax stock no. 022071)⁷⁷ to generate heterozygous Cd4:Cre+/dCas9-KRAB+/Foxp3-eGFP+ or Cd4:Cre+/dCas9-p300+/Foxp3-eGFP+ experimental mice. Spleens and lymph nodes were collected, dissociated and processed with ammonium chloride potassium (ACK) lysis buffer and passed through the Magnisort Mouse CD4 T cell Enrichment Kit (Thermo Fisher, cat. no. 8804-6821-74). Lymphocytes were surface-stained with antibodies for the purification of Tn cells (CD4+CD25-CD62LhiCD44ho) through FACS using either a Beckman Culture Astiros (CD4-FITC 1:400, CD25-eFluor450 1:300, CD62L-APC 1:500, CD44-PE 1:500, and fixable viability dye e780 1:1,000) or a SONY SH800 instrument (CD4-PECy7 1:500, CD25-PE 1:500, CD44-FITC 1:400, CD62L-PEcy5 1:500, Live/Dead Red 1:1,000) to achieve ≥98% purity. The antibodies were obtained from eBioscience (CD4, cat. no. 25-0042-82; CD25, cat. no. 12-0251-83; CD44, cat. no. 11-0441-85; CD62L, cat. no. 15-0621-82). For ChIP-seq, the Tn cells were purified using the Magnisort Mouse Naïve CD4+ T cell Enrichment Kit (Thermo Fisher, cat. no. 8804-6824-74) instead of sorting, to increase the starting material.

In vitro culture conditions for CD4 T cell subset polarization. All T-cell polarizations were performed using Olympus tissue-culture plastic that had been coated with anti-Hamster IgG (20 ng μl^{-1} , MP Biomedical, cat. no. 856984) and kept at 37 °C for at least 4h beforehand. Th cells were seeded at ~250,000 cells ml $^{-1}$. The Th0-activating culture medium consisted of hamster-anti-CD3e (0.25 μg ml $^{-1}$), hamster-anti-CD28 (1 μg ml $^{-1}$), the blocking antibodies anti-IL-4 (2 μg ml $^{-1}$, eBioscience, cat. no. 16-7041-85) and anti-IFN- γ (2 μg ml $^{-1}$, eBioscience, cat. no. 16-7311-85), and mIL-2 (10 ng ml $^{-1}$, Peprotech, cat. no. 212-12). The iT $_{\rm reg}$ cell-polarizing culture medium contained the above and was supplemented with hTGF β 1 (5 ng ml $^{-1}$, eBioscience, cat. no. 14-8348-62).

T-cell retroviral transduction and in vitro culture. The Tn cells were isolated and purified from the spleen and lymph nodes of \$Cd4:Cre^+/dCas9-p300^+/Foxp3-eGFP^+\$ or \$Cd4:Cre^+/dCas9-KRAB^+\$ mice via FACS as described above and cultured in ThO-activating culture conditions at 37 °C and 5% CO2. Between 20 and 24 h later, the activated T cells were transduced via spinfection with viral supernatant containing 6.66 ng ml⁻¹ polybrene and Mouse Stem Cell Virus (MSCV) encoding the \$Foxp3\$ gRNA-5 promoter-targeting gRNA, or a non-targeting control gRNA. Viral supernatant was replaced with ThO or iT_{reg} cell media and the cells were cultured for 7 or 3 d for p300 and KRAB experiments, respectively.

Purification of p300-induced T_{reg} effector cells for co-culture. At 7 d after viral transduction, T_{reg} effector cells were stained with fixable viability dye e780 (eBioscience, cat. no. 65-0865-18) and Thy1.1 (CD90.1-PE, StemCell, cat. no. 60024PE, 1:400). Viable transduced cells expressing FOXP3-eGFP were FACS purified (Thy1.1+/FOXP3-eGFP+) and resuspended at 500,000 cells ml $^{-1}$ in RPMI.

Purification of p300-induced T_{reg} effector T cells for ChIP and RNA-seq. Tn cells were activated for 20–24h in Th0 conditions as above before transduction with Foxp3 or control gRNA. At 3 d after transduction, 100,000 or 2 million viable, Thy1.1+ transduced T cells were FACS purified for RNA-seq or ChIP-seq, respectively.

Purification of conventional T cells and suppression assay. Spleens and lymph nodes from Foxp3-eGFP mice (JAX stock no. 006769) were processed as above and the recovered splenocytes were stained for viability (Live/Dead Red, Thermo Fisher, cat. no. L34971, 1:1,000) and with anti-CD4-PE-Cy7 (1:500). CD4+FOXP3-eGFP- live cells were purified using a SONY SH800 FACS machine. Cells were washed with 30 ml PBS and stained with 5 μ M Cell Trace Violet (Thermo Fisher, cat. no. C34557) following the manufacturer's instructions. Stained conventional T cells were diluted to 500,000 cells ml⁻¹ in RPMI and co-cultured with 25,000 T_{reg} cells per well for 72 h with 25,000 anti-CD3/ anti-CD28 Dynabeads (Thermo Fisher, cat. no. 11161). Cells were then removed from the magnetic beads, stained for viability with e780 and processed for flow cytometric analysis.

FOXP3 protein staining and flow cytometry analysis. For dCas9^{KRAB}-based experiments, in vitro cultured, transduced T cells were stained with anti-Thy1.1-PerCP-Cy5.5 (eBioscience, cat. no. 45-0900-82, 1:300) and Fixable Viability Dye eFluor780 (1:1,000) prior to fixation and permeabilization with FOXP3 Transcription Factor Staining Buffer Kit (eBioscience, cat. no. 00-5523-00) following the manufacturer's protocol. Cells were stained intracellularly with anti-FOXP3-PE (eBioscience, cat. no. 12-5773-82, 1:200) and data were collected with a BD FACSCanto II cytometer using FACSDiva v8.0.3. All flow cytometry was analyzed using FlowJo v10.6.2

Statistics and reproducibility. No statistical method was used to predetermine the sample size. Sample sizes were chosen to be consistent with other published reports of dCas9-based activators and repressors used in vivo^{21,28,29}. In each of these three studies, n=3 or 4 was used in the majority of assays that measured changes in gene expression. For high-throughput sequencing-based assays, sample sizes were chosen to be consistent with ENCODE standards All statistical analysis was conducted using Prism v6 or v9 (GraphPad), with the exception of Supplementary Fig. 2, which was analyzed using R v3.5.1. Sequencing data were excluded only if they failed to pass pre-existing criteria for technical quality. RT-qPCR data were excluded only if our control for RNA collection and sample processing showed an abnormally low yield, defined as more than 2 s.d. from the mean of the sample set. Electrophysiology data were excluded only if the measurement of basal membrane properties suggested that the cell was dying. Mice for all experiments were selected randomly with respect to parent of origin, age and sex, with the exception of mice for stereotaxic injections, for which only adult male animals were used. Sample collection and analysis for liver-targeted experiments were performed blind. Animals were injected, numbered and housed mixed in cages, and samples were collected based on animal number only. Sample collection and analysis for T-cell, neuron and brain experiments were not performed blind.

Reporting Summary. Further information on research design is available in the Nature Research Reporting Summary linked to this article.

Data availability

Raw sequencing files are available from the NCBI Gene Expression Omnibus via SuperSeries accession GSE146848. Source data are provided with this paper.

Code availability

Data processing and analysis code is made available through Zenodo 80 and on GitHub (https://github.com/ReddyLab/gemberling-et-al-NMETH-A42509C).

References

- Springer, M. L., Rando, T. A. & Blau, H. M. Gene delivery to muscle. Curr. Protoc. Hum. Genet. Chapter 13, Unit13.4 (2002).
- Salmon, P. & Trono, D. Production and titration of lentiviral vectors. *Curr. Protoc. Neurosci.* Chapter 4, Unit 4.21 (2006).
- Morita, S., Kojima, T. & Kitamura, T. Plat-E: an efficient and stable system for transient packaging of retroviruses. Gene Ther. 7, 1063–1066 (2000).
- Bolger, A. M., Lohse, M. & Usadel, B. Trimmomatic: a flexible trimmer for Illumina sequence data. *Bioinformatics* 30, 2114–2120 (2014).
- 64. Dobin, A. et al. STAR: ultrafast universal RNA-seq aligner. *Bioinformatics* 29, 15–21 (2013).
- Harrow, J. et al. GENCODE: the reference human genome annotation for The ENCODE Project. Genome Res. 22, 1760–1774 (2012).
- Liao, Y., Smyth, G. K. & Shi, W. The Subread aligner: fast, accurate and scalable read mapping by seed-and-vote. *Nucleic Acids Res.* 41, e108 (2013).
- Love, M. I., Huber, W. & Anders, S. Moderated estimation of fold change and dispersion for RNA-seq data with DESeq2. Genome Biol. 15, 550 (2014).
- 68. Stephens, M. False discovery rates: a new deal. Biostatistics 18, 275-294 (2017).
- Li, B. & Dewey, C. N. RSEM: accurate transcript quantification from RNA-Seq data with or without a reference genome. BMC Bioinformatics 12, 323 (2011).
- Savic, D., Gertz, J., Jain, P., Cooper, G. M. & Myers, R. M. Mapping genome-wide transcription factor binding sites in frozen tissues. *Epigenetics Chromatin* 6, 30 (2013).
- Langmead, B., Trapnell, C., Pop, M. & Salzberg, S. L. Ultrafast and memory-efficient alignment of short DNA sequences to the human genome. *Genome Biol.* 10, R25 (2009).
- Ramirez, F., Dundar, F., Diehl, S., Gruning, B. A. & Manke, T. deepTools: a flexible platform for exploring deep-sequencing data. *Nucleic Acids Res.* 42, W187–W191 (2014).
- Zhang, Y. et al. Model-based analysis of ChIP-Seq (MACS). Genome Biol. 9, R137 (2008)
- Quinlan, A. R. & Hall, I. M. BEDTools: a flexible suite of utilities for comparing genomic features. *Bioinformatics* 26, 841–842 (2010).
- Haribhai, D. et al. Regulatory T cells dynamically control the primary immune response to foreign antigen. J. Immunol. 178, 2961–2972 (2007).
- Lin, W. et al. Regulatory T cell development in the absence of functional Foxp3. Nat. Immunol. 8, 359–368 (2007).

- 77. Lee, P. P. et al. A critical role for Dnmt1 and DNA methylation in T cell development, function, and survival. *Immunity* 15, 763–774 (2001).
- 78. Landt, S. G. et al. ChIP-seq guidelines and practices of the ENCODE and modENCODE consortia. *Genome Res.* 22, 1813–1831 (2012).
- Conesa, A. et al. A survey of best practices for RNA-seq data analysis. Genome Biol. 17, 13 (2016).
- Barrera, A. ReddyLab/gemberling-et-al-NMETH-A42509C: NMETH-A42509C-v1.0. (2021). https://doi.org/10.5281/zenodo.4777237

Acknowledgements

We thank J. Deng and B. Ryu for assistance with viral injections, and K. Franks for his support in performing the electrophysiology recordings. This work has been supported by the Allen Distinguished Investigator Program through The Paul G. Allen Frontiers Group to C.A.G., Translating Duke Health Initiative to K.D.P., Open Philanthropy to C.A.G., National Institutes of Health (NIH) grants R33DA041878 to A.E.W. and C.A.G., R01DA036865 to C.A.G., U01A1146356 to C.A.G., UM1HG009428 to T.E.R., M.C. and C.A.G., UG3AR075336 to A.A., and R01GM115474 to M.C., National Science Foundation (NSF) grant EFMA-1830957 to C.A.G., Defense Advanced Research Projects Agency (DARPA) grant HR0011-19-2-0008 to C.A.G., a Pfizer-NCBiotech Distinguished Postdoctoral Fellowship in Gene Therapy to J.C.B., and a Swiss National Science Foundation Postdoctoral Fellowship to V.C.

Author contributions

M.P.G., K.S., E.R., K.R.T.-E., F.L., A.K., V.C., M.F.H., L.C.B., C.A.W. and J.C.B. conducted experiments and analyzed data. H.D., D.C.R. and L.L. assisted with the mouse

experiments. A.B. and K.S. performed ChIP-Seq and RNA-seq analysis. M.P.G., K.S., A.E.W. and C.A.G. wrote portions of the paper. I.B.H. provided critical reagents. V.J.M. and A.A. produced AAV9 for the mouse experiments. M.C., K.D.P., T.E.R., A.E.W. and C.A.G. provided guidance on the experimental design and interpretation of results. All authors edited the text.

Competing interests

C.A.G., I.B.H. and T.E.R. have filed patent applications related to CRISPR technologies for genome engineering. C.A.G. is an advisor to Tune Therapeutics, Sarepta Therapeutics, Levo Therapeutics and Iveric Bio, and a co-founder of Tune Therapeutics, Element Genomics and Locus Biosciences. A.A. is a co-founder of and advisor to StrideBio and TorqueBio. T.E.R. is a co-founder of Element Genomics. M.P.G. is a co-founder and employee of Tune Therapeutics. All other authors have no competing interests.

Additional information

Supplementary information The online version contains supplementary material available at https://doi.org/10.1038/s41592-021-01207-2.

Correspondence and requests for materials should be addressed to C.A.G.

Peer review information *Nature Methods* thanks Randall J. Platt and the other, anonymous, reviewer(s) for their contribution to the peer review of this work. Madhura Mukhopadhyay was the primary editor on this article and managed its editorial process and peer review in collaboration with the rest of the editorial team.

Reprints and permissions information is available at www.nature.com/reprints.

nature research

corresponding author(s):	Charles Gerspach
Last updated by author(s):	Apr 27, 2021

Reporting Summary

Nature Research wishes to improve the reproducibility of the work that we publish. This form provides structure for consistency and transparency in reporting. For further information on Nature Research policies, see our <u>Editorial Policies</u> and the <u>Editorial Policy Checklist</u>.

<u> </u>					
St	. ລ	1	IC.	ŀι	\sim
- 1 I	$\overline{}$				ι.

For	all st	atistical analyses, confirm that the following items are present in the figure legend, table legend, main text, or Methods section.
n/a	Cor	nfirmed
	\boxtimes	The exact sample size (n) for each experimental group/condition, given as a discrete number and unit of measurement
	X	A statement on whether measurements were taken from distinct samples or whether the same sample was measured repeatedly
	\boxtimes	The statistical test(s) used AND whether they are one- or two-sided Only common tests should be described solely by name; describe more complex techniques in the Methods section.
	X	A description of all covariates tested
	\boxtimes	A description of any assumptions or corrections, such as tests of normality and adjustment for multiple comparisons
	\boxtimes	A full description of the statistical parameters including central tendency (e.g. means) or other basic estimates (e.g. regression coefficient AND variation (e.g. standard deviation) or associated estimates of uncertainty (e.g. confidence intervals)
	\boxtimes	For null hypothesis testing, the test statistic (e.g. <i>F</i> , <i>t</i> , <i>r</i>) with confidence intervals, effect sizes, degrees of freedom and <i>P</i> value noted <i>Give P values as exact values whenever suitable.</i>
\boxtimes		For Bayesian analysis, information on the choice of priors and Markov chain Monte Carlo settings
X		For hierarchical and complex designs, identification of the appropriate level for tests and full reporting of outcomes
\boxtimes		Estimates of effect sizes (e.g. Cohen's d, Pearson's r), indicating how they were calculated
		Our web collection on statistics for biologists contains articles on many of the points above.

Software and code

Policy information about availability of computer code

Data collection

ImageLab 5.2.1 - Western blot imaging CFX manager 3.0 - Biorad CFX qPCR machine Biotek Gen5.0 - software for plate reader LiCor image studio 4.0 - western blot imaging Sony SH800s software v2.1.5 - Sony cell sorter BD FACSDiva v8.0.3 WaveMetrics IgorPro 6.22A AxographX v1.7.6 Neuromatic v3.0 ImageJ 1.46j

Data analysis

Prism 6.0.0, Prism 9.0.0- graphs and statistics Microsoft Excel - data analysis Flowjo 10.6.2 - flow analysis R v3.5.1 - data analysis and visualization Python v2.7.11 - data visualization pandas v0.23.3 seaborn v0.9.0 subread package v1.4.6-p4 bedtools2 v2.25.0 MACS2 v2.1.1.20160309

Picard MarkDuplicates v1.130 deeptools bamCoverage (v3.0.1)

Bowtie v1.0.0

RSEM v1.2.21
Trimmomatic v0.32
DESeq2 (v1.22.0)
STAR v2.4.1a
FastQC v0.11.2

For manuscripts utilizing custom algorithms or software that are central to the research but not yet described in published literature, software must be made available to editors and reviewers. We strongly encourage code deposition in a community repository (e.g. GitHub). See the Nature Research guidelines for submitting code & software for further information.

Data

Policy information about availability of data

All manuscripts must include a data availability statement. This statement should provide the following information, where applicable:

- Accession codes, unique identifiers, or web links for publicly available datasets
- A list of figures that have associated raw data
- A description of any restrictions on data availability

ChIP and RNA-seq data sets generated during this study are available on GEO in both raw and processed forms (GSE146848). Figures 1, 3, and 4, and supplemental figures 3, 4, 5, 6, 10, 11, and 13. Other data can be made available on request.

				C·			4.0	
-10	\Box	I-sn	ല	TIC	rer	۱Or	TIN	σ
	ı U	l-sp	CCI	110	1 $^{\circ}$		CITI	Ъ

Please select the one below that is the best fit for your research. If you are not sure, read the appropriate sections before making your selection.					
X Life sciences	Behavioural & social sciences	Ecological, evolutionary & environmental sciences			
For a reference copy of the document with all sections, see <u>nature.com/documents/nr-reporting-summary-flat.pdf</u>					
Life sciences study design					

Life sciences study design

All studies must disclose on these points even when the disclosure is negative.

Sample size

No statistical method was used to predetermine samples size. For CRISPR-based assays, sample sizes were chosen to be in line with other published reports of Cas9 and dCas9 based activators and repressors used in vivo9, 25, 26. In each of these three studies, n=3 or 4 were used in the majority of assays measuring changes in gene expression. For high-throughput sequencing based assays, sample sizes were chosen to be in line with ENCODE standards27, 28.

Data exclusions

Data are only excluded for failing to pass pre-existing criteria for technical quality. RT-PCR data were excluded only if our control for RNA harvesting and sample processing showed abnormally low yield, defined as more than 2 standard deviations from the mean of the sample set. Electrophysiology data were excluded only if the measurement of basal membrane properties suggested that the cell was dying.

Replication

All experiments have been replicated successfully in at least at least two independent biological replicates.

Randomization

Mice for all experiments were selected randomly with respect to parent of origin, age (between 8-12 weeks old) and sex with the exception of mice for sterotaxic injections for which only adult male animals were used.

Blinding

Sample collection and analysis for PDX1 and PCSK9 experiments were performed blind. Animals were injected, numbered, and housed mixed in cages and samples were collected based on animal number only. Sample collection and analysis for T cell and neuron experiments were not performed blind.

Reporting for specific materials, systems and methods

We require information from authors about some types of materials, experimental systems and methods used in many studies. Here, indicate whether each material, system or method listed is relevant to your study. If you are not sure if a list item applies to your research, read the appropriate section before selecting a response.

Materials & experimental systems	Methods		
n/a Involved in the study	n/a Involved in the study		
Antibodies	ChIP-seq		
Eukaryotic cell lines	Flow cytometry		
Palaeontology and archaeology	MRI-based neuroimaging		
Animals and other organisms	·		
Human research participants			
Clinical data			
Dual use research of concern			
•			

Alltibodies

Antibodies used

Supplier Product Cat# Lot(s)# Clone Dilution Website

clone-ox-7.html#section-data-and-publications

Cell Signaling Anti-Gapdh 2118L 10 1:5000 https://www.cellsignal.com/products/primary-antibodies/gapdh-14c10-rabbit-mab/2118 Abcam Anti-LDLR ab52818 GR274869-6 1:1000 https://www.abcam.com/ldl-receptor-antibody-ep1553y-ab52818.html

EMD Millipore Anti-Actin MAB1501 2908073 1:5000 https://www.emdmillipore.com/US/en/product/Anti-Actin-Antibody-clone-C4,MM NF-MAB1501

Sigma Anti-Rabbit HRP A6154 SLBP3451V 1:5000 https://www.sigmaaldrich.com/catalog/product/sigma/a6154?lang=en®ion=US Santa Cruz Anti-Mouse HRP sc-2005 1:5000 https://www.scbt.com/p/goat-anti-mouse-igg-hrp

Biotium Goat anti-mouse 680 20253 18C1127 1:5000 https://biotium.com/product/goat-anti-mouse-igg1/

Life Techniologies Goat Anti-Rabbit IgG AlexaFluor 488 A27034 2069632 1:200 https://www.thermofisher.com/antibody/product/Goat-anti-Rabbit-IgG-H-L-Secondary-Antibody-Recombinant-Polyclonal/A27034

MP Biomedical anti-Hamster IgG 856984 08112; 7606 1:50 https://www.mpbio.com/us/0856984-goat-affinity-purified-antibody-to-hamster-igg-whole-molecule

Abcam Pdx1 ab47267 2069632 1:200 https://www.abcam.com/pdx1-antibody-ab47267.html

EnCor Biotechnology Anti-Cas9 MCA-3F 60216 1:2000 https://encorbio.com/product/mca-3f9/

EnCor Biotechnology Rabbit anti-Cas9 RPCA-CAS9-Sp 51816 1:1000 https://encorbio.com/product/rpca-cas9-sp/Calbiochem Anti-c-Fos PC38 D00100487 1:1000 https://www.labome.com/product/EMD-Millipore/PC38-100UL.html

Jackson immunoresearch Goat Anti-Rabbit Cy3 711-165-152 70667 1:500 https://www.jacksonimmuno.com/catalog/products/711-165-152

Cell Signaling Anti-Cre recombinase 15036 1 1:300 https://www.cellsignal.com/products/primary-antibodies/cre-recombinase-d7l7l-xp-rabbit-mab/15036

Diagenode Cas9 C15200229-100 2 5ug https://www.diagenode.com/en/p/crispr-cas9-monoclonal-antibody-100-ug Sigma Flag-M2 F1804 SLCG2330; SLBT7654 5ug https://www.sigmaaldrich.com/catalog/product/sigma/f1804?lang=en®ion=US Abcam H3K27ac ab4729 GR3231988-1 5ug https://www.abcam.com/histone-h3-acetyl-k27-antibody-chip-grade-ab4729.html Abcam H3K9me3 ab8898 GR3244172-1 5ug https://www.abcam.com/histone-h3-tri-methyl-k9-antibody-chip-grade-ab8898.html StemCell Technologies Anti-Rat CD90.1 (Thy1.1) 60024PE BX35382 OX-7 1:400 https://www.stemcell.com/anti-rat-cd90-antibody-

eBioscience Anti-Mouse/Rat CD90.1 (Thy1.1), PerCP-Cyanine5.5 45-0900-82 4341934 HIS51 1:300 https://www.thermofisher.com/antibody/product/CD90-1-Thy-1-1-Antibody-clone-HIS51-Monoclonal/45-0900-82

eBioscience Anti-Mouse CD4 PE-Cyanine7 25-0042-82 1994141 RM4-5 1:500 https://www.thermofisher.com/antibody/product/CD4-Antibody-clone-RM4-5-Monoclonal/25-0042-82

eBioscience Anti-Mouse CD4 FITC 25-0041-82 4329631 GK1.5 1:400 https://www.thermofisher.com/antibody/product/CD4-Antibody-clone-GK1-5-Monoclonal/25-0041-82

eBioscience Anti-Mouse CD25 PE 12-0251-83 4300552 PC61.5 1:500 https://www.thermofisher.com/antibody/product/CD25-Antibody-clone-PC61-5-Monoclonal/12-0251-82

eBioscience Anti-Mouse CD25 e450 48-0251-82 2011204 PC61.5 1:300 https://www.thermofisher.com/antibody/product/CD25-Antibody-clone-PC61-5-Monoclonal/48-0251-82

eBioscience Anti-Mouse CD44 FITC 11-0441-85 1943165 IM7 1:400 https://www.thermofisher.com/antibody/product/CD44-Antibody-clone-IM7-Monoclonal/11-0441-82

eBioscience Anti-Mouse CD44 PE 12-0441-82 4330029 IM7 1:500 https://www.thermofisher.com/antibody/product/CD44-Antibody-clone-IM7-Monoclonal/12-0441-82

eBioscience Anti-Mouse CD62L APC 17-0621-82 4318204 MEL-14 1:500 https://www.thermofisher.com/antibody/product/CD62L-L-Selectin-Antibody-clone-MEL-14-Monoclonal/17-0621-82

eBioscience Anti-Mouse CD62L PE-Cyanine5 15-0621-82 1931486 MEL-14 1:500 https://www.thermofisher.com/antibody/product/CD62L-L-Selectin-Antibody-clone-MEL-14-Monoclonal/15-0621-82

eBioscience Anti-Mouse/Rat Foxp3 PE 12-5773-82 210594 FJK-16s 1:200 https://www.thermofisher.com/antibody/product/FOXP3-Antibody-clone-FJK-16s-Monoclonal/12-5773-82

eBioscience Anti-Mouse CD28 Functional Grade Purified 16-0281-86 2211008 37.51 1:1000 https://www.thermofisher.com/antibody/product/CD28-Antibody-clone-37-51-Monoclonal/16-0281-82

eBioscience Anti-Mouse CD3e Functional Grade Purified 16-0031-86 2009296 145-2C11 1:4000 https://www.thermofisher.com/antibody/product/CD3e-Antibody-clone-145-2C11-Monoclonal/16-0031-82

eBioscience Anti-Mouse IFN-gamma Functional Grade Purified 16-7311-85 2269979 XMG1.2 1:500 https://www.thermofisher.com/antibody/product/IFN-gamma-Antibody-clone-XMG1-2-Monoclonal/16-7311-81

 $eBioscience\ Anti-Mouse\ Il-4\ Functional\ Grade\ Purified\ 16-7041-85\ 2197861\ 11B11\ 1:500\ https://www.thermofisher.com/antibody/product/Il-4-Antibody-clone-11B11-Monoclonal/16-7041-81$

Validation

All antibodies were validated with negative control samples included in all analyses. Websites are listed following each antibody below:

Cell Signaling Anti-Gapdh https://www.cellsignal.com/products/primary-antibodies/gapdh-14c10-rabbit-mab/2118

Abcam Anti-LDLR https://www.abcam.com/ldl-receptor-antibody-ep1553y-ab52818.html

EMD Millipore Anti-Actin https://www.emdmillipore.com/US/en/product/Anti-Actin-Antibody-clone-C4,MM_NF-MAB1501

 $Sigma\ Anti-Rabbit\ HRP\ https://www.sigmaaldrich.com/catalog/product/sigma/a6154?lang=en\®ion=US$

Santa Cruz Anti-Mouse HRP https://www.scbt.com/p/goat-anti-mouse-igg-hrp

Biotium Goat anti-mouse 680 https://biotium.com/product/goat-anti-mouse-igg1/

Life Techniologies Goat Anti-Rabbit IgG AlexaFluor 488 https://www.thermofisher.com/antibody/product/Goat-anti-Rabbit-IgG-H-L-Secondary-Antibody-Recombinant-Polyclonal/A27034

 $MP\ Biomedical\ anti-Hamster\ IgG\ https://www.mpbio.com/us/0856984-goat-affinity-purified-antibody-to-hamster-igg-whole-molecule$

Abcam Pdx1 https://www.abcam.com/pdx1-antibody-ab47267.html

EnCor Biotechnology Anti-Cas9 https://encorbio.com/product/mca-3f9/

 ${\tt EnCor\ Biotechnology\ Rabbit\ anti-Cas9\ https://encorbio.com/product/rpca-cas9-sp/}$

Calbiochem Anti-c-Fos https://www.labome.com/product/EMD-Millipore/PC38-100UL.html

```
Jackson immunoresearch Anti-Rabbit Cy3 https://www.jacksonimmuno.com/catalog/products/711-165-152
```

Cell Signaling Anti-Cre recombinase https://www.cellsignal.com/products/primary-antibodies/cre-recombinase-d7l7l-xp-rabbit-

Diagenode Cas9 https://www.diagenode.com/en/p/crispr-cas9-monoclonal-antibody-100-ug

Sigma Flag-M2 https://www.sigmaaldrich.com/catalog/product/sigma/f1804?lang=en®ion=US

Abcam H3K27ac https://www.abcam.com/histone-h3-acetyl-k27-antibody-chip-grade-ab4729.html

Abcam H3K9me3 https://www.abcam.com/histone-h3-tri-methyl-k9-antibody-chip-grade-ab8898.html

StemCell Technologies Anti-Rat CD90.1 (Thy1.1) https://www.stemcell.com/anti-rat-cd90-antibody-clone-ox-7.html#section-dataand-publications

eBioscience Anti-Mouse/Rat CD90.1 (Thy1.1), PerCP-Cyanine5.5 https://www.thermofisher.com/antibody/product/CD90-1-Thy-1-1-Antibody-clone-HIS51-Monoclonal/45-0900-82

eBioscience Anti-Mouse CD4 PE-Cyanine7 https://www.thermofisher.com/antibody/product/CD4-Antibody-clone-RM4-5-Monoclonal/25-0042-82

eBioscience Anti-Mouse CD4 FITC https://www.thermofisher.com/antibody/product/CD4-Antibody-clone-GK1-5-

Monoclonal/25-0041-82 eBioscience Anti-Mouse CD25 PE https://www.thermofisher.com/antibody/product/CD25-Antibody-clone-PC61-5-

Monoclonal/12-0251-82

eBioscience Anti-Mouse CD25 e450 https://www.thermofisher.com/antibody/product/CD25-Antibody-clone-PC61-5-Monoclonal/48-0251-82

eBioscience Anti-Mouse CD44 FITC https://www.thermofisher.com/antibody/product/CD44-Antibody-clone-IM7-Monoclonal/11-0441-82

eBioscience Anti-Mouse CD44 PE https://www.thermofisher.com/antibody/product/CD44-Antibody-clone-IM7-Monoclonal/12-0441-82

eBioscience Anti-Mouse CD62L APC https://www.thermofisher.com/antibody/product/CD62L-L-Selectin-Antibody-clone-MEL-14-Monoclonal/17-0621-82

eBioscience Anti-Mouse CD62L PE-Cyanine5 https://www.thermofisher.com/antibody/product/CD62L-L-Selectin-Antibody-clone-MFI-14-Monoclonal/15-0621-82

eBioscience Anti-Mouse/Rat Foxp3 PE https://www.thermofisher.com/antibody/product/FOXP3-Antibody-clone-FJK-16s-Monoclonal/12-5773-82

eBioscience Anti-Mouse CD28 Functional Grade Purified https://www.thermofisher.com/antibody/product/CD28-Antibodyclone-37-51-Monoclonal/16-0281-82

eBioscience Anti-Mouse CD3e Functional Grade Purified https://www.thermofisher.com/antibody/product/CD3e-Antibodyclone-145-2C11-Monoclonal/16-0031-82

eBioscience Anti-Mouse IFN-gamma Functional Grade Purified https://www.thermofisher.com/antibody/product/IFN-gamma-Antibody-clone-XMG1-2-Monoclonal/16-7311-81

eBioscience Anti-Mouse IL-4 Functional Grade Purified https://www.thermofisher.com/antibody/product/IL-4-Antibodyclone-11B11-Monoclonal/16-7041-81

Eukaryotic cell lines

Policy information about cell lines

Cell line source(s)

PLAT-E cells were from Dan Littman (NYU), HEK293T cells were from ATCC (CRL-11268)

Authentication

PLAT-E cells were not authenticated in our lab and taken in good faith. HEK293T cells were authenticated by ATCC. Both of these cell lines were not used to collect data but only produce Retro and Lentivirus for downstream applications.

Mycoplasma contamination

Cell lines were not tested for mycoplasma contamination

Commonly misidentified lines (See ICLAC register)

Name any commonly misidentified cell lines used in the study and provide a rationale for their use.

Animals and other organisms

Policy information about studies involving animals; ARRIVE guidelines recommended for reporting animal research

Laboratory animals

Mouse Line Strain Jack Stock Number Strain of Origin Backcrossing Information

Rosa26-LSL-dCas9-p300 C57BL/6N (Jax Stock No: 033065) (129S6/SvEvTac x C57BL/6NCrl) N5?+N6

Rosa26-LSL-dCas9-KRAB C57BL/6N (Jax Stock No: 033066) (129S6/SvEvTac x C57BL/6NCrl) N3?+N6

CD4Cre C57BL/6J (Jax Stock No: 022071) (C57BL/6 x DBA/2) N13+F5

B6-Foxp3-eGFP C57BL/6J (Jax Stock No: 006772) (129X1/SvJ) N5?+N3F6

CD4:Cre-Rosa26-LSL-dCas9-p300-Foxp3-eGFP C57BL/6JN N/A (C57BL/6 x DBA/2) x (129X1/SvJ) x (129S6/SvEvTac x C57BL/6NCrl) N6 CD4:Cre-Rosa26-LSL-dCas9-KRAB-Foxp3-eGFP C57BL/6JN N/A (C57BL/6 x DBA/2) x (129X1/SvJ) x (129S6/SvEvTac x C57BL/6NCrl) N6

dCas9-effector mice were generated by electroporating a modified pAi9 targeting vector into hybrid G4 B6N/129S6 ES cells to target transgenic insertion into the ROSA locus. Positive clones were expanded and injected into the 8-cell morulae of ICR mice. Chimeric mice were then mated to establish the transgenic line.

For T cell experiments, the resulting Rosa26-LSL-dCas9-p300 or Rosa26-LSL-dCas9-KRAB mice above were backcrossed with a B6-Foxp3EGFP mouse line (Jax stock# 006772) for at least 6 generations and then crossed with B6-CD4:Cre (Jax stock# 022071) to generate either Cd4:Cre+/dCas9-KRAB+/Foxp3-eGFP+ or Cd4:Cre+/dCas9-p300+/Foxp3-eGFP+.

All mice were used between 8-12 weeks old and not selected based on specific sex, with the exception of those adult males used only for sterotaxic injection experiments.

Wild animals No wild animals were used in these studies

Field-collected samples

There were no field-collected samples used in this study.

Ethics oversight

All experiments involving animals were conducted with strict adherence to the guidelines for the care and use of laboratory animals of the National Institute of Health (NIH). All experiments were approved by the Institutional Animal Care and Use Committee (IACUC) at Duke University.

Note that full information on the approval of the study protocol must also be provided in the manuscript.

ChIP-sea

Data deposition

Confirm that both raw and final processed data have been deposited in a public database such as GEO.

Confirm that you have deposited or provided access to graph files (e.g. BED files) for the called peaks.

Data access links

May remain private before publication.

GSE146848 - https://www.ncbi.nlm.nih.gov/geo/query/acc.cgi?acc=GSE146848 Reviewer Token: slcpiqaejnuvjcd

Files in database submission

mmLiver_p300.Cas9.PBS.rep10 mmLiver p300.Cas9.PBS.rep11 mmLiver_p300.Cas9.PBS.rep12 mmLiver_p300.Cas9.PBS.rep4 mmLiver p300.Cas9.controlgRNA.rep1 mmLiver_p300.Cas9.controlgRNA.rep2 mmLiver_p300.Cas9.controlgRNA.rep3 mmLiver_p300.Cas9.controlgRNA.rep5 mmLiver_p300.Cas9.Pdx1.rep6 mmLiver_p300.Cas9.Pdx1.rep7 mmLiver_p300.Cas9.Pdx1.rep8 mmLiver_p300.Cas9.Pdx1.rep9 mmLiver p300.input.PBS.rep10 mmLiver_p300.input.PBS.rep11 mmLiver_p300.input.PBS.rep12 mmLiver p300.input.PBS.rep4 mmLiver p300.input.controlgRNA.rep1 mmLiver_p300.input.controlgRNA.rep2 mmLiver_p300.input.controlgRNA.rep3 mmLiver_p300.input.controlgRNA.rep5 mmLiver_p300.input.Pdx1.rep6 mmLiver_p300.input.Pdx1.rep7 mmLiver_p300.input.Pdx1.rep8 mmLiver p300.input.Pdx1.rep9 mmLiver p300.K27ac.PBS.rep10 mmLiver_p300.K27ac.PBS.rep11 mmLiver p300.K27ac.PBS.rep12 mmLiver_p300.K27ac.PBS.rep4 mmLiver p300.K27ac.controlgRNA.rep1 mmLiver_p300.K27ac.controlgRNA.rep2 mmLiver_p300.K27ac.controlgRNA.rep3 mmLiver p300.K27ac.controlgRNA.rep5 mmLiver_p300.K27ac.Pdx1.rep6 mmLiver_p300.K27ac.Pdx1.rep7 mmLiver p300.K27ac.Pdx1.rep8 mmLiver p300.K27ac.Pdx1.rep9 mmLiver KRAB.flag.PBS.rep12 mmLiver_KRAB.flag.PBS.rep1 mmLiver_KRAB.flag.PBS.rep2 mmLiver KRAB.flag.PBS.rep4 mmLiver KRAB.flag.controlgRNA.rep10 mmLiver_KRAB.flag.controlgRNA.rep11 mmLiver_KRAB.flag.controlgRNA.rep8 mmLiver_KRAB.flag.controlgRNA.rep9 mmLiver_KRAB.flag.Pcsk9.rep3 mmLiver KRAB.flag.Pcsk9.rep5 mmLiver_KRAB.flag.Pcsk9.rep6 mmLiver_KRAB.flag.Pcsk9.rep7 mmLiver_KRAB.input.PBS.rep12 mmLiver_KRAB.input.PBS.rep1 mmLiver KRAB.input.PBS.rep2 mmLiver KRAB.input.PBS.rep4 mmLiver_KRAB.input.controlgRNA.rep10

```
mmLiver_KRAB.input.controlgRNA.rep11
mmLiver\_KRAB.input.controlgRNA.rep8
mmLiver KRAB.input.controlgRNA.rep9
mmLiver KRAB.input.Pcsk9.rep3
mmLiver KRAB.input.Pcsk9.rep5
mmLiver_KRAB.input.Pcsk9.rep6
mmLiver_KRAB.input.Pcsk9.rep7
mmLiver KRAB.K9me3.PBS.rep12
mmLiver KRAB.K9me3.PBS.rep1
mmLiver_KRAB.K9me3.PBS.rep2
mmLiver KRAB.K9me3.PBS.rep4
mmLiver_KRAB.K9me3.controlgRNA.rep10
mmLiver_KRAB.K9me3.controlgRNA.rep11
mmLiver KRAB.K9me3.controlgRNA.rep8
mmLiver KRAB.K9me3.controlgRNA.rep9
mmLiver_KRAB.K9me3.Pcsk9.rep3
mmLiver_KRAB.K9me3.Pcsk9.rep5
mmLiver_KRAB.K9me3.Pcsk9.rep6
mmLiver_KRAB.K9me3.Pcsk9.rep7
mmCD4.CREneg.g5.K27ac.rep1
mmCD4.CREneg.g5.K27ac.rep2
mmCD4.CREneg.g5.K27ac.rep3
mmCD4.CREpos.g5.K27ac.rep1
mmCD4.CREpos.g5.K27ac.rep2
mmCD4.CREpos.g5.K27ac.rep3
mmCD4.CREpos.NTC.K27ac.rep1
mmCD4.CRFpos.NTC.K27ac.rep2
mmCD4.CREpos.NTC.K27ac.rep3
```

Genome browser session (e.g. <u>UCSC</u>)

http://trackhub.genome.duke.edu/reddylab/collab/matt_p300_krab/hub.txt

Methodology

Replicates

All replicates refer to individual mice either dCas9-p300 and dCas9-KRAB. We collected 4 mice (biological replicates) per treatment, with an average Spearman correlation coefficient ranging from 70-95%.

Sequencing depth

Across experiments, on average 39M reads were sequenced per replicate (Cl 13.4M-71.5M). From those, 30.4M unique mapped reads were recorded on average (Cl 9.5M-56.9M). All libraries were sequenced in an Illumina HiSeq4000 or NextSeq platform, and the runs were configured as 51SE (51bp single-end) or 25PE (25bp paired-end) respectively

Antibodies

Cas9 (Diagenode C15200229-100), Flag-M2 (Sigma, F1804), H3K27ac (Abcam, ab4729), or H3K9me3 (Abcam, ab8898)

Peak calling parameters

Peak calling was performed using MACS2 (see version number in methods), using the appropriate input controls (--control parameter) and the additional following parameters: --no-model -g mm --extsize <SPP_FRAG_LENGTH_ESTIMATION>. The fragment length estimation is calculated using the run_spp.R script provided by Anshul Kundaje. See Software for more details.

Data quality

We ran strand cross-correlation analyses for all our samples to ensure the associated values of Relative and Normalized Strand Cross-correlation were within the acceptable ranges. Additionally, we computed the Non-redundant Read Fraction (NRF) and the Fraction of Reads in Peaks (FRiP) which showed values within range. For ChIP-seq samples of Cas9 and FLAG, some of these metrics didn't seem to apply given the extremely low expected number of peaks. For those, we relied on Spearman correlation analysis for 10kb bins across the mouse genome.

Software

We used the CWL pipeline from the GGR project to process these samples, which has been described in a previous publication (PMID: 30097539). All the code is publicly available and can be found in github: https://github.com/Duke-GCB/GGR-cwl/tree/master/v1.0

Flow Cytometry

Plots

Confirm that:

- \square The axis labels state the marker and fluorochrome used (e.g. CD4-FITC).
- The axis scales are clearly visible. Include numbers along axes only for bottom left plot of group (a 'group' is an analysis of identical markers).
- All plots are contour plots with outliers or pseudocolor plots.
- A numerical value for number of cells or percentage (with statistics) is provided.

Methodology

Sample preparation

Spleens and lymphnodes were harvested, dissociated, and processed with ammonium chloride potassium (ACK) lysis buffer and enriched with a Magnisort mouse CD4 T cell enrichment kit (eBioscience cat# 8804-6821-74)

Instrument

FACS was performed using either a Beckman Culture Astiros or or SONY SH800S; Flow cytometry analysis was performed using either a BD FACSCanto II cytometer or SONY SH800S in analyzer mode.

Software

BD FACSDiva software was used to collect samples from the Beckman Culture Astiros cell sorter and BD FACSCanto II cytometer. The SH800S software was used to collect samples from the SONY SH800S cell sorter and analyzer. FlowJo v10 was used to analyze the .fcs files. Prism6 or Prism9 and Illustrator 2020 was used to prepare figures for publication

Cell population abundance

all naive T cells were collected in a single sort with a final purity of ≥98% from the Beckman Culture Astiros and ≥95% from the SONY SH800S

Gating strategy

Gating strategy for

- 1) naive T cell sorts: Lymphocytes/Single Cells/Live cells/CD4+/CD25-/CD62L+/CD44lo
- 2) CRISPR activation and interference experiments: Lymphocytes/Single Cells/Live cells/THY1.1+/FOXP3+
- 3) Suppression Assays: Lymphocytes/Single Cells/Live cells/Cell Trace Violet+ (CTV+)

| Tick this box to confirm that a figure exemplifying the gating strategy is provided in the Supplementary Information.